A Tsunami Forecast Model For Bar Harbor, Maine

Stewart Allen

Table of Contents

List of Tables iii

List of Figures iv

Abstract 1

1.0 Background and Objectives 1

2.0 Forecast Methodology 2

3.0 Model Development 3

4.0 Results and Discussion 7

5.0 Summary and Conclusions 11

6.0 Acknowledgments 12

7.0 References 12

Appendix A 31

Appendix B. Propagation Database: Atlantic Ocean Unit Sources. 32

Appendix C Description of Indices 43

C.1 Normalised error in the maximum amplitude 43

C.2 Pearson correlation coefficient 43

C.3 Normalised Root-mean-square error 44

C.4 Index of Agreement 44

C.5 Watterson's transformed Mielke index 44

C.6 Mielke and Berry index 45

Appendix D. SIFT Testing 46

D.1. TESTING PROCEDURE 46

D.2 Results 48

List of Tables

Table 1: Tidal characteristics for the Bar Harbor tide gauge. 15

Table 2: MOST setup parameters for reference and forecast models for Bar Harbor, Maine. 16

Table 3: Synthetic tsunami events. The location of sources 1-5 and 7 are shown in Figure 8. 17

Table 4: Values of various indices for each of the seven synthetic scenarios considered and the micro synthetic scenario. A description of the indices is given in Appendix C. 17

Table 5. Earthquake parameters for Atlantic Source Zone unit sources. 34

Table 6. Earthquake parameters for South Sandwich Islands unit sources.....41

Table 7. table of maximum and minimum amplitudes (cm) at the Bar harbor, Maine warning point for synthetic events tested using SIFT 3.2 and obtained during development. 49

List of Figures

Figure 1: Contour relief of the Gulf of Maine. The features labeled are (a) the Gulf of Maine, (b) The Georges Bank (c) The Northeast Channel and (d) The Great South Channel. These features are referenced in the text. The red cross indicates the approximate location of Bar Harbor. Depths are in meters. 18

Figure 2: Contour relief of Frenchman bay. Units are in meters. The features labeled are (a) Bar Harbor township, (b) Long Porcupine Island, (c) Burnt Porcupine Island (d) Sheep Porcupine Island, (e) Bar Island, (f) Bald Porcupine Island (Note the breakwater extending east.), (g) Cromwell Cove (h) outflow region from Eddie Brook and (i) Hulls Cove. These features are referenced in the text. The red cross indicates the location of the tide gauge and depths are in meters. 18

Figure 3: Aerial photography of the Bar Harbor region. Key land features are labeled. Taken from Google Earth. 19

Figure 4: Oblique aerial view of the Bar Harbor region. Photograph by Flicker user Smudge 9000, used under Creative Commons Attribution 2.0. 19

Figure 5: Instrument housing for the Bar Harbor tide gauge. 20

Figure 6: A depiction of the extent and location of the forecast grids, including how each is nested. The top-left figure shows the extent of the A reference grid. The top-right figure shows this grid in more detail with the extent of the A forecast grid shown by the yellow rectangle and the extent of the B reference grid shown by the red rectangle. The other figures follow in a similar manner. Note that there is no yellow rectangle depicting the extent of the C forecast grid, since it covers the same areas as the C reference grid. 20

Figure 7: Comparison of the C reference grid (left) with the C forecast grid. Depths are in meters. 21

Figure 8: An example of some of the effects of necessary bathy modifications on the C forecast grid in the vicinity of Bar Harbor (the

unmodified bathymetry is shown on the left). Note the changes to the breakwater and the area near the tide gauge (marked by the red cross). The effects of smoothing over the entire grid are also apparent on the form of the (underwater) contours.....21

Figure 9: Location of Caribbean unit sources. The synthetic scenarios used in this study consist of scaling and combining these unit sources. The unit sources that make up each scenario are colored according to the key. The single unit source that comprises scenario 7 is also used by scenario 2. 22

Figure 10: Location of the South Sandwich Sources. As in Figure 9, the unit sources that make up each scenario are colored according to the key. 22

Figure 11: Plot of maximum amplitude for both the forecast and reference C grids for the micro scenario. Units are in cm and the magenta cross shows the location of the tide gauge.....23

Figure 12: Time series of sea-level elevations at the forecast and reference grid nodes nearest the Bar Harbor tide gauge for the micro scenario. The series from the forecast grid is shown in in red and the series for the reference model is shown in black. Units are in cm. The length of both series is 12 hours, calculated from when the tsunami first reaches the edge of the respective A grids.....23

Figure 13: Plot of maximum amplitude for both the forecast and reference C grids for the scenario 1. Units are in cm and the magenta cross shows the location of the tide gauge. 24

Figure 14: Time series of sea-level elevations at the forecast and reference grid nodes nearest the Bar Harbor tide gauge for scenario 1. The series from the forecast grid is shown in in red and the series for the reference model is shown in black. Units are in cm. 24

Figure 15: Plot of maximum amplitude for both the forecast and reference C grids for the scenario 2. Units are in cm and the magenta cross shows the location of the tide gauge. 25

Figure 16: Time series of sea-level elevations at the forecast and reference grid nodes nearest the Bar Harbor tide gauge for scenario 2. The series from the forecast grid is shown in in red and the series for the reference model is shown in black. Units are in cm. 25

Figure 17: Plot of maximum amplitude for both the forecast and reference C grids for the scenario 3. Units are in cm and the magenta cross shows the location of the tide gauge. 26

Figure 18: Time series of sea-level elevations at the forecast and reference grid nodes nearest the Bar Harbor tide gauge for scenario 3. The series from the forecast grid is shown in in red and the series for the reference model is shown in black. Units are in cm. 26

Figure 19: Plot of maximum amplitude for both the forecast and reference C grids for the scenario 4. Units are in cm and the magenta cross shows the location of the tide gauge. 27

Figure 20: Time series of sea-level elevations at the forecast and reference grid nodes nearest the Bar Harbor tide gauge for scenario 4. The series from the forecast grid is shown in in red and the series for the reference model is shown in black. Units are in cm. 27

Figure 21: Plot of maximum amplitude for both the forecast and reference C grids for the scenario 5. Units are in cm and the magenta cross shows the location of the tide gauge. 28

Figure 22: Time series of sea-level elevations at the forecast and reference grid nodes nearest the Bar Harbor tide gauge for scenario 5. The series from the forecast grid is shown in in red and the series for the reference model is shown in black. Units are in cm. 28

Figure 23: Plot of maximum amplitude for both the forecast and reference C grids for the scenario 6. Units are in cm and the magenta cross shows the location of the tide gauge. 29

Figure 24: Time series of sea-level elevations at the forecast and reference grid nodes nearest the Bar Harbor tide gauge for scenario 6.

The series from the forecast grid is shown in in red and the series for the reference model is shown in black. Units are in cm. 29

Figure 25: Plot of maximum amplitude for both the forecast and reference C grids for the scenario 7. Units are in cm and the magenta cross shows the location of the tide gauge. 30

Figure 26: Time series of sea-level elevations at the forecast and reference grid nodes nearest the Bar Harbor tide gauge for scenario 7. The series from the forecast grid is shown in in red and the series for the reference model is shown in black. Units are in cm. 30

Figure 27. Atlantic Source unit sources 33

Figure 28. South Sandwich Islands Subduction Zone.....40

Figure 29: Response of the Bar Harbor forecast model to synthetic scenario ATSZ 38-47 (alpha=25). Maximum sea surface elevation for (a) A-grid, b) B-grid, c) C-grid. Sea surface elevation time series at the C-grid warning point (d) The lower time series plot is the result obtained during model development and is shown for comparison with test results.....50

Figure 30: Response of the Bar Harbor forecast model to synthetic scenario ATSZ 48-57 (alpha=25). Maximum sea surface elevation for (a) A-grid, b) B-grid, c) C-grid. Sea surface elevation time series at the C-grid warning point (d) The lower time series plot is the result obtained during model development and is shown for comparison with test results.....51

Figure 31: Response of the Bar Harbor forecast model to synthetic scenario SSSZ 1-10 (alpha=25). Maximum sea surface elevation for (a) A-grid, b) B-grid, c) C-grid. Sea surface elevation time series at the C-grid warning point (d) The lower time series plot is the result obtained during model development and is shown for comparison with test results.....52

Abstract

As part of NOAA's tsunami forecast system, this study addresses the development, validation, and stability tests of a tsunami forecast model for Bar Harbor, Maine. Based on the Method of Splitting Tsunami (MOST), the tsunami forecast model is constructed at a spatial resolution of approximately 50 m in the finest grid to accomplish a 4-hour simulation of wave inundation onto dry land within 20 minutes of CPU time. A reference inundation model is developed in parallel, using grid size up to 17 meters to provide a reference for the forecast model.

Due to lack of historical tsunami data, the accuracy and stability of the forecast model were evaluated using eight synthetic scenarios generated in the Puerto Rico Trench, Hispaniola Trench, Cayman Trough, Los Muertos Trough and South Sandwich Island at magnitudes ranging from Mw 7.5 to Mw 9.3. The results show that the forecast model performs well at reproducing the characteristics simulated in the high-resolution reference model. However, although it consistently matches the character of the resolution model, it tends to under-predict the amplitude of the reference model. This implies that the forecast model is predisposed to underestimating the potential impacts (from a forecast perspective) in the regions of interest.

The results indicate that Bar Harbor and certain surrounding localities may suffer impact (including some inundation) in the event of some very large tsunamis. The regions surrounding the narrow, intertidal channel between Bar Harbor and Bar Island is particularly at risk, along with the region at the mouth of Eddie Brook, Hulls Cove and Cromwell Cove. Time series show that tsunami energy often does not quickly attenuate over time, meaning that dangerous conditions may persist for many hours following arrival of the initial tsunami.

1.0 Background and Objectives

The Pacific Marine Environmental Laboratory (PMEL) of the National Oceanic and Atmospheric Administration (NOAA) Center for Tsunami Research (NCTR) has developed a tsunami forecasting capability for operational use by NOAA's Tsunami Warning Centers located in Hawaii and Alaska (Titov et al. 2005). The system is designed to efficiently provide basin-wide warning of approaching tsunami waves. The system, termed Short-term Inundation Forecast of Tsunamis (SIFT), combines real-time tsunami event data with numerical models to produce estimates of tsunami arrival times, amplitudes and inundations at coastal communities of interest. The SIFT system integrates several key components: deep-ocean, real-time observations of tsunamis, a basin-wide pre-computed propagation database (Gica, et al., 2009) of water level and flow velocities based

on potential seismic unit sources, an inversion algorithm to refine the tsunami source based on deep-ocean observations during an event, and optimized tsunami forecast models.

Bar Harbor is a coastal town of the state of Maine and is situated on the North Eastern shore of Mount Desert Island. As of the 2009 US census[1], It had approximately 5200 inhabitants. It is a popular summer holiday destination and during that period, its population swells to tens-of-thousands of inhabitants[2]. The nearby Arcadia National Park, which surrounds Bar Harbor and incorporates several nearby islands, receives an estimated 2 million visitors annually[3]. The relatively sheltered, natural waters of Frenchman Bay mean that recreational maritime activities are also prevalent in Bar Harbor with many cruise ships visiting each year. It is this popularity as a tourist destination and the prevalence of recreational maritime activities in its vicinity, as to why Bar Harbor was selected for the construction of a tsunami forecast model.

This report details the development of a high-resolution tsunami forecast model for Bar Harbor. It includes a description of the development of the bathymetric grids, followed by stability testing and model validation with a set of synthetic events (given the absence of historical data).

2.0 Forecast Methodology

A high-resolution inundation model is used as the basis for development of a tsunami forecast model to operationally provide estimates of wave arrival time, wave height, and inundation at Bar Harbor, Maine following tsunami generation. All tsunami forecast models are run in real time while a tsunami is propagating across the open ocean. The Bar Harbor model was designed and tested to perform under stringent time constraints given that time is generally the single limiting factor in saving lives and property. The goal of this work is to maximize the length of time that the community of Bar Harbor has to react to a tsunami threat by providing accurate information quickly to emergency managers and other officials responsible for warning the community and protecting infrastructure.

The general tsunami forecast model, based on the Method of Splitting Tsunami (MOST), is used in the tsunami inundation and forecasting system to provide real-time tsunami forecasts at selected coastal communities. The model runs in minutes while employing high-resolution grids constructed by the National Geophysical Data Center (NGDC). The Method of Splitting Tsunami (MOST) is a suite of numerical simulation codes capable of simulating three processes of tsunami evolution: generation by earthquake, transoceanic propagation, and inundation of dry land. The MOST model has been extensively tested against a

[1] http://www.census.gov/popest/data/index.html
[2] http://www.barharbormaine.gov/xhtml/121/ViewDefault/
[3] http://www.nps.gov/acad/parkmgmt/statistics.htm

number of laboratory experiments and benchmarks (Synolakis et al., 2008) and was successfully used for simulations of many historical tsunami events. The main objective of a forecast model is to provide an accurate, yet rapid, estimate of wave arrival time, wave height, and inundation in the minutes following a tsunami event. Titov and González (1997) describe the technical aspects of forecast model development, stability, testing, and robustness, and Tang et al. (2009) provide detailed forecast methodology.

A basin-wide database of pre-computed water elevations and flow velocities for unit sources covering worldwide subduction zones has been generated to expedite forecasts (Gica et al., 2008). As the tsunami wave propagates across the ocean and successively reaches tsunameter observation sites, recorded sea level is ingested into the tsunami forecast application in near real-time and incorporated into an inversion algorithm to produce an improved estimate of the tsunami source. A linear combination of the pre-computed database is then performed based on this tsunami source, now reflecting the transfer of energy to the fluid body, to produce synthetic boundary conditions of water elevation and flow velocities to initiate the forecast model computation.

Accurate forecasting of the tsunami impact on a coastal community largely relies on the accuracies of bathymetry and topography and the numerical computation. The high spatial and temporal grid resolution necessary for accurate modeling poses a challenge to the run-time requirement for real-time forecasts. Each forecast model consists of three telescoped grids with increasing spatial resolution to the finest grid, and temporal resolution for simulation of wave inundation onto dry land. The forecast model utilizes the most recent bathymetry and topography available to reproduce the correct wave dynamics during the inundation computation. Forecast models, including the Bar Harbor model, are constructed for at-risk populous coastal communities in the Pacific and Atlantic Oceans. Previous and present development of forecast models in the Pacific (Titov et al., 2005; Titov, 2009; Tang et al., 2008; Wei et al., 2008) have validated the accuracy and efficiency of each forecast model currently implemented in the real-time tsunami forecast system. Models are tested when the opportunity arises and are used for scientific research. Tang et al. (2009) provide forecast methodology details.

3.0 Model Development

Modeling of coastal communities is accomplished by development of a set of three nested grids that telescope down from a large spatial extent to a grid that finely defines the localized community. The basis for these grids is a high-resolution digital elevation model constructed by either NCTR or, more commonly, by NGDC using best available bathymetric, topographic, and coastal shoreline data for an at-risk community. For each community, data are compiled from a variety of sources to produce a digital elevation model referenced to Mean High Water in the vertical and to the World Geodetic System 1984 in the

horizontal[4]. From these digital elevation models, a set of three high-resolution reference models are constructed and then "optimized" to run within an operationally specified period of time (specifically 4 hours of simulation should be completed within 10 minutes of wall-clock time).

3.1. Forecast Area

The local bathymetry of the region surrounding Bar Harbor is relatively complex. The region is situated within the Gulf of Maine, which is approximately 420 km (260 miles) wide at its mouth and approximately 200 km (125 miles) deep. The gulf is entirely on the North American eastern continental shelf, which is relatively wide, extending on the order of 320 to 440 km (200 to 275 miles) from the coastline in this region. Water depths beyond the continental shelf rise from approximately 5000m to 2000m near the continental margin. On the shelf, water depths are approximately 100 to 200 m in the Gulf of Maine. However, there is an elevated region, the Georges Bank, situated near the shelf edge. It is 240 km (50 miles) in length and 120 km (75 miles) in width and is submerged to depths ranging from several meters to several dozen meters. This feature affords a degree of protection to the Gulf of Maine from incoming tsunamis. There are two deeper channels at either end of the Georges Bank, the Northeast Channel (200 to 250 m or 650 to 820 ft deep) and the Great South Channel (50 to 100 m or 160 to 320 ft deep). A map of the Gulf of Maine, with key features indicated is shown in Figure 1.

Bar Harbor is located on the western shores of Frenchman Bay, which, in turn, is located on the northern shores of the Gulf of Maine. The mouth of Frenchman Bay is approximately 8 km (5 miles) wide and it maintains roughly this width over its 15 km (9 miles) length. Bar Harbor is located approximately 8 km (5 miles) from the bay mouth. A map of Frenchman Bay, with key features indicated, is shown in Figure 2 and an aerial view of the region is shown in Figure 3. An oblique view of Bar Harbor and surrounds is shown in Figure 4.

There are many islands of varying size within Frenchman Bay. Those of most significance to Bar Harbor are known as the Porcupine Group and consists of 5 main islands and several smaller outcrops. In particular, the southern most island of the group, known as Bald Porcupine Island, features an artificial breakwater. Constructed in 1917, it extends southwest from the island some 800 meters (2600 feet) towards the coast, leaving a narrow, shallow channel 200m (700 feet) wide. On the eastern side of Bald Porcupine island, there is a deeper, wider channel that is around 1600 m (1 mile) wide and as deep as 70m (230 ft).

Bar Harbor itself is tucked away in a narrow channel 500m (188ft) wide to the south of Bar Island. The waters of this channel are very shallow, being mostly less than 5m (16ft ft) in depth. At the western end of this channel, there is a natural, intertidal sand bar connecting Bar Harbor and Bar Island (although recall

[4] http://ngdc.noaa.gov/mgg/inundation/tsunami/inundation.html

that this study is conducted using a digital elevation model referenced to Mean High Water, meaning this sand bar remains submerged in the model). There are a number of artificial structures within Bar Harbor that have been constructed to support recreational maritime activities. Some of these are solid (i.e. neither on footings nor are floating) and are large enough to be resolved by the tsunami model.

3.2. Historical Events and Tide Gauge Records

There is a tide gauge located on a pier in Bar Harbor. The gauge is owned and operated by the National Ocean Service, who has assigned the gauge assigned reference identifiers of ATGM1/8413320. It was established in August 1947 with its present instrumentation installed in June 1999. It has verified hourly records going back to March 1950. Characteristics of the tide gauge are given in Table 1 and a photo of the instrumentation housing is shown in Figure 5. The location of the gauge is indicated on Figure 2 and this point will serve as the warning point for the models. The coordinates of the grid node in each model that is nearest to the tide gauge's location is also given in Table 1.

Though tsunamis have occurred in the Atlantic basin in the past, generated both seismically and by other mechanisms, there have been no historical observations of tsunamis by the Bar Harbor tide gauge. Therefore, this model will be evaluated using solely synthetic tsunami events.

3.3. Model Setup

The general methodology for modeling at-risk coastal communities is to develop a set of three nested grids, referred to as the A-, B-, and C-grids, each of which becomes successively finer in resolution as they telescope into the population and economic center of the community of interest. The offshore area is covered by the largest and lowest resolution A-grid while the near-shore details are resolved within the finest scale C-grid to the point that tide gauge observations recorded during historical tsunamis (where available) are resolved within expected accuracy limits.

The procedure is to begin development with large spatial extent merged bathymetric and topographic grids at high resolution. The basis for these grids is a high-resolution digital elevation model constructed by NGDC and NCTR using all available bathymetric, topographic, and shoreline data to reproduce the wave dynamics during the inundation computation for an at-risk community. Data were compiled from a variety of sources to produce a digital elevation model referenced to Mean High Water in the vertical and to the World Geodetic System 1984 in the horizontal[5]. Full details of the development are contained in Friday et al. (2011). The author considers it to be an adequate representation of the local topography/bathymetry. As new digital elevation models become available,

[5] http://ngdc.noaa.gov/mgg/inundation/tsunami/inundation.html

forecast models will be updated and report updates will be posted at http://nctr.pmel.noaa.gov/forecast_reports/.

From this digital elevation model, a set of three high-resolution, 'reference grids' are constructed for development of a high-resolution 'reference model'. On the basis of past validation and verification studies of the MOST model, many of which use a model set up similar to that described here, this reference model serves as our experimental control.

From the reference model, a further set of grids are constructed, which constitute an 'optimized' model. The term 'optimized is used here in that these grids are constructed by sub-sampling of the reference model to coarsen the resolution and shrink the overall grid dimensions. This is done with the aim that the optimized model will run within an operationally specified period of time (usually a 4 hour simulation of modeled tsunami waves within 10 minutes of wall-clock time). This model will henceforth be referred to as the 'optimized tsunami forecast model' or 'forecast model' for brevity.

Table 2 provides specific details of both reference and tsunami forecast model grids, including extents. Complete input parameter information for the model runs is provided in Appendix A. The locations of the grids, including a depiction of how they are nested, are shown in Figure 6.

The A-grid in the reference model is identical to the grid used in the reference model developed for Portland, Maine (Spillane, 2009). This grid is relatively large, in order to contain the entire Gulf of Maine, the George Bank, the continental margin and outlying deep oceanic waters. It is important these coastal bathymetric features be entirely encapsulated within the grid so that shoaling of tsunamis, as they propagate from deep waters onto the continental shelf, and subsequent changes to the waveforms are well characterized.

The A-grid in the forecast model was designed at the same resolution, but optimized so that its southern boundary is closer to the continental margin. By moving the boundary in this manner, the deepest water depths contained within the grid are reduced, which allows a larger time-step to be used, but without inducing numerical instability[6]. The eastern and western boundaries were also shifted to exclude shallow waters that are not close to the area of interest (see Figure 6, top-right). Coarser resolutions for the A-forecast grid were also tested with a view to further increasing the computation speed. However, these were shown to not accurately match the simulations produced by the reference model. Compared to other tsunami forecast models developed by PMEL, the A-grid in the Bar Harbor forecast model is very large. However, this is necessary since the continental shelf is very wide in the region of interest.

[6] In this context, instability is of the type generated when the Courant-Friedrichs-Lewy condition is not met.

Given the relative complexity of the coastline in this region, the B-grid of the reference model was chosen roughly centered on Frenchman Bay and extended to encompass all coastal waters surrounding Mt Desert Island roughly 50km (31 miles) in each direction. The B-grid of the forecast model was constructed at a resolution coarser than its reference model counterpart, as well as covering a smaller area (see Figure 6, bottom right). The C-grids were chosen centered on Bar Harbor and so that the grid boundaries do not intersect any of the nearby islands of Frenchman Bay. Both grids cover the same area, but the C-forecast grid is at a coarser resolution (Figure 7).

For both models, the grids required some modification in order to obtain numerically stable solutions. These modifications included some manipulations over the entirety of each grid. Algorithms that identify and reduce any regions of excessive steepness, as well as those that 'smooth' extremely fine-scale features were employed. Without application of these tools, such geographic features may generate numerical instabilities.

Further modifications were performed over localized coastal regions. This was usually achieved by manually changing the elevation of individual grid points so that they were made to be above sea level. This technique was employed to deal with grid points where instabilities were generated only in locations well away from Bar Harbor (e.g. on the B-grids or near the edge of the C-grids).

In other places, modifications were made to improve the representation of specific features, particularly in the C-forecast grid. The relatively low resolution of this grid means that the breakwater extending from Bald Porcupine Island is not entirely resolved. Therefore, grid points were manually modified to make the breakwater artificially wide so that it was complete and unbroken along its length.

Another manual modification was made to the C-forecast grid in the vicinity of the tide gauge. The narrow peninsula immediately to the east of the tide gauge location was only 1-grid node in width. Also, the grid node nearest to the tide gauge location was extremely shallow (less than 1 meter in depth). The algorithm within the MOST model cannot handle such narrow geographic features and so the width of this peninsula was increased by 1 node on the eastern side (i.e. the opposite side to the tide gauge location) and the grid point closest to the tide gauge was deepened slightly. An example of the effects of these localized modifications, as well as those applied to the entire grid, can be seen in Figure 8.

4.0 Results and Discussion

The accuracy of the forecast model was tested using 8 hypothetical tsunami scenarios. These scenarios were constructed from SIFT Propagation database (Gica et al., 2008) using from unit sources located in the Caribbean region (shown in Figure 9) and the South Sandwich Islands region (not shown). Unit sources in the database were scaled and combined to make larger tsunami

sources for a series of ‘synthetic scenarios’. The linear combination based on these tsunami sources is taken from the pre-computed database to produce synthetic boundary conditions of water elevation and flow velocities for the forecast and reference model computations. Parameters for the synthetic scenarios are listed in Table 3.

The first stability test of the models was to simulate a very small tsunami. A single unit source in the South Sandwich Islands region was scaled by a factor of 0.5 (equivalent to a magnitude 7.3 earthquake) and used produce a so-called ‘micro scenario’, the location of which is indicated in Figure 10. Testing with this scenario ensures that no instability or other spurious oscillations arise in the models when they are largely unperturbed.

Six more scenarios (5 in the Caribbean, 1 in the South Sandwich Islands) were constructed by linearly combining multiple (20 in each scenario) magnitude 7.5 unit sources. The resultant sources form a series of mega-tsunami scenarios, each equivalent to a magnitude 9.3 earthquake. These will be termed scenarios 1 to 5 (Caribbean) and scenario 6 (South Sandwich Islands). The locations of the unit sources that are combined to make each of scenarios 1 through 5 are indicated in Figure 9 while the location of scenario 6 is indicated in Figure 10. Testing with these very large magnitude scenarios ensure the models are stable under extreme forcing.

A seventh scenario was constructed from a single magnitude 7.5 unit source in the Caribbean. Though much less severe, this source tests the stability of the model using a scenario reflective an earthquake in this region that has a much shorter return period than the mega tsunami cases. The unit source used for scenario 7 is also indicated on Figure 9.

4.1. Results from the Synthetic Micro Scenario

Plots of the maximum amplitude for the forecast and reference C-grids are shown in Figure 11 and time series of sea-level elevations at the tide gauge location are shown in Figure 12. The plots show that in the absence of significant forcing, the models remain unperturbed. Figure 12 does display some very small oscillations in both time series. However, they do not grow larger than approximately 1 mm and so we can be confident that both models do not generate any numerical instability.

4.2. Results from Other Synthetic Scenarios

Results from the other scenarios are displayed as maximum amplitude plots and time series from Figure 13 through to Figure 26. The time series are taken from the grid node nearest the tide gauge location. Various indices that indicate the degree of agreement have been calculated for the time series for each scenario. A description of these indices is included in Appendix C and the results are included in included in Table 4.

All scenarios, except scenario 7, display a good agreement between the forecast and reference model and even scenario 7 still shows reasonable agreement (this is discussed in more detail below). In all cases, the forecast model captures the character of the reference model well, but has an overall tendency to under-predict.

Perhaps the most significant scenarios are scenarios 1 and 2, since they are, by far, the largest scenarios, in terms of the amplitudes observed over the grids and at the tide gauges. These scenarios show some inundation of low-lying areas, particularly scenario 2. In these cases, the forecast model time series displays a good match to the reference model, a notion supported by Table 4. This match is best over the period of time immediately following the tsunami arrival. After approximately two hours, the models diverge slightly, as amplitudes in the forecast model begin to be under-predicted compared to the reference model (this appears to be slightly worse in scenario 1). It is important to note that in both cases, large values occur throughout the entire time series. Scenario 2, in particular, displays very large values towards the end of the calculated series. These large values likely result from waves arriving at the tide gauge following reflections from regional and remote bathymetric features. The coarse resolution of the forecast model appears to generate less inundation of coastal areas in scenarios 1 and 2 (a clear example of this can be seen in Figure 15 in the vicinity of the Bar Harbor township).

Scenario 5 arguably shows the best agreement between the forecast and reference models among all scenarios. The time series Figure 22 show a high degree of correlation and the values of the indices in Table 4 are the second highest of all scenarios, after scenario 4. However, the fields of maximum amplitude presented in Figure 21 provide arguably the best match of all scenarios, in terms of the patterns and amplitudes. Closer examination of Figure 22 shows that the time series closely match from the time of arrival (approximately 5 hours after initialization) through the following 2.5 hours. After this time, the forecast model simulates the low-frequency variability well but has larger errors in the high-frequency oscillations. The largest value in the reference model time series occurs at the end of the displayed time series and the forecast model appears to underestimate this peak. However, in this case, the forecast model is late in predicting this peak and so occurs just beyond the time period covered by Figure 22. The actual maximum value predicted by the forecast model is within one centimeter of that predicted by the reference model.

The results for scenario 4 present an unusual case. The time series in Figure 20 shows the highest degree of agreement of all scenarios, and this is confirmed by the values of the indices in Table 4. Yet unlike the other scenarios, the series are largely devoid of any high-frequency oscillations. Furthermore, the plot of maximum amplitudes in Figure 19 shows that for this scenario, the forecast model tends to over predict compared to the reference model. This behavior is unique among the scenarios considered in this report.

Scenario 6 is unique in that it is the only case (other than the micro scenario) with sources not located in the Caribbean. It also shows some unique behavior in its time series (Figure 24). While the other 'mega' tsunami scenarios (1-5) show a distinct low-frequency component, scenario 6 is devoid of such oscillations. Furthermore, well after the arrival of the tsunami, the high-frequency oscillations present grow appreciably. It is not clear whether this amplification is due to local dynamics around Bar Harbor or later boundary forcing (perhaps due to reflection of wave in the Atlantic Ocean basin). However, what is most important is that the forecast model is able to capture this behavior, with the indices indicating a level of agreement as high as the other scenarios. Like the other scenarios, the time series (Figure 24) shows that the forecast model tends to under-predict the reference model and this behavior is also very apparent in the fields of maximum amplitude (Figure 23).

The smallest scenario considered here, scenario 7, is the scenario where the forecast model most poorly reproduces the reference model. As in all other scenarios, there is initially good agreement between time series of the models (Figure 26), but after approximately 1 hour, they begin to diverge. Initially, the amplitudes of the forecast model decrease, while there is some growth in the reference model. However, later into the series, the oscillations also become out of phase. Table 4 also shows that the forecast model does a relatively poorly at simulating the reference model with the lowest scores for all indices. Likewise, the plots of maximum amplitude show notable differences (Figure 25). This case is instructive as it demonstrates how even in the absence of significant forcing (as in, overall variations are small, compared to other scenarios), the interactions at the coast are relatively important. In other words, the differences between the forecast and reference models in this scenario are relatively large for scenario 7.

There are some consistent features among the scenarios. The time series plots show that despite its differences from the reference model, the forecast model simulates the arrival time of tsunamis at the Bar Harbor tide gauge location well. The initial waves following arrival match well and the model also retains the low-frequency character of the reference model. However, high-frequency oscillations tend to be attenuated after 1-4 hours. It is suggested that this is the reason that the forecast model also tends to underestimate the peak amplitude of the reference model (a feature not only apparent the times series, but also in the maximum amplitude plots). Further experiments with the forecast model grids suggest this is primarily due to the coarser resolution of the B- and C-grids. However, the reduced spatial extent of the A- and B-grids is a secondary contributing factor.

Another key feature of tsunami behavior in the Bar Harbor region is the persistence of tsunami energy, as revealed by the time series. All cases show oscillations that persist throughout the time series. In some cases, this may result from local effects, such as local bathymetry. However, in other cases, it is may arise from waves arriving at Bar Harbor following reflections from regional (i.e. within the outer model grids) or even distant bathymetric features (such as the

African coastline). Specifically arrival of later waves may occur in scenarios 2, 4, 5 and 6, since they show an increase in sea-level amplitude (and sometimes even the maximum value) well after the initial arrival. These characteristics is important for warning guidance, as they indicate that in in the event of a tsunami affecting Bar Harbor, dangerous conditions may persist for many hours following arrival of the initial tsunami.

The maximum amplitude plots for scenario 1 and 2 (Figure 13 and Figure 15 respectively) do show patterns, by way of large sea level amplitudes and inundation, that suggest the regions surrounding Bar Harbor where tsunami impact may be greatest. These at risk regions, indicated in Figure 2, include the shallow channel and sand bar between Bar Harbor and Bar Island, the region at the mouth of Eddie Brook, Hulls Cove and Cromwell Cove. Some other coves to the south of Cromwell Cove also experience impact by. Of these areas, the Eddie Brook region and Hulls Cove experience the greatest impact, with the largest values for smaller scenarios such as scenarios 6 and 7, being observed in the maximum amplitude plots in these regions.

It was mentioned in section 3.3 that the forecast model should be designed to run within a operationally specified period of time, specifically 4 hours of simulation should be completed within 10 minutes of wall-clock time. Table 2 states that the forecast model for Bar Harbor does not run within this time, but instead completes 4 hours of tsunami simulation in 21 minutes. Tests show that this relatively slow speed is due to the large forecast A-grid, which is required to adequately simulate the transmission of tsunamis onto the very wide continental shelf present in this region. However, it should be noted that the speed of the Bar Harbor Forecast model is similar to other models developed for the Atlantic Basin for use with SIFT (e.g. Wei, 2010). Moreover, Bar Harbor's distant proximity from potential tsunamigenic sources means that forecast model's speed is still sufficient to complete a simulation for use in supplying forecast and warning guidance.

5.0 Summary and Conclusions

This report outlines the steps take to generate a tsunami forecast model for Bar Harbor, Maine. An outline of the steps taken to produce the bathymetric grids was provided. In the absence of any historical records of past tsunami events in the Atlantic basin, the resulting model was tested using a series of synthetic scenarios.

The scenarios revealed that the low-resolution forecast model performs well at reproducing the characteristics simulated in the high-resolution reference model. However, although it consistently matches the character of the resolution model, it tends to under-predict the amplitude of the reference model. This implies that the forecast model is predisposed to underestimating the potential impacts in the regions of interest (from a forecast perspective).

These issues may be alleviated by future revisions of the forecast model. As computing power increases and model technology improves, the resolution of the forecast grids may be increased, while still maintaining computation speeds that are within or reasonably close to the target run-time. Increasing the spatial extent of the grids may also improve the forecast model's accuracy.

The results also indicate that Bar Harbor and certain surrounding localities may suffer impact in the event of some very large tsunamis. The regions surrounding the narrow, intertidal channel between Bar Harbor and Bar Island is particularly at risk, along with the region at the mouth of Eddie Brook, Hulls Cove and Cromwell Cove. Time series show that tsunami energy often does not quickly attenuate over time, meaning that dangerous conditions may persist for many hours following arrival of the initial tsunami.

6.0 Acknowledgments

Assistance with the development of this model was gratefully received from Diego Arcas, Yong Wei, Edison Gica, Mick Spillane, Elena Tolkova and Marie Eble.

The image used for Figure 4 was accessed from Flickr.com and is attributed to user Smudge 9000. It used under the Creative Commons Attribution 2.0. Figure 3 was taken from Google Earth.

This publication is partially funded by the Joint Institute for the study of the Atmosphere and Ocean (JISAO) under NOAA Cooperative Agreement No. NA17RJ1232, JISAO Contribution No. XXXX. This is PMEL Contribution No. NNNN

7.0 References

Allen, S.C.R and D.J.M. Greenslade (2012): Indices for the Objective Assessment of Tsunami Forecast Models. Pure Appl. Geophys., doi: 10.1007/s00024-012-0522-4

Friday, D.Z, L.A. Taylor, B.W. Eakins, K.S. Carignan, P.R. Grothe, E. Lim, and M.R. Love, (2011): Digital Elevation Models of Bar Harbor, Maine: Procedures, Data Sources and Analysis, NOAA National Geophysical Data Center technical report, Boulder, CO, 22 pp.

Gica, E., M. Spillane, V.V. Titov, C. Chamberlin, and J.C. Newman (2008): Development of the forecast propagation database for NOAA's Short-term Inundation Forecast for Tsunamis (SIFT). NOAA Tech. Memo. OAR PMEL-139, 89 pp.

Mielke, P.W., Jr. (1984): Meteorological applications of permutation techniques based on distance functions. In Krishnaiah, P.R. and Sen, P. K. (eds.), Handbook of Statistics, Vol 4, Elsevier, Amsterdam, 813-830.

Mielke, P.W., Jr. and Berry, K.J. (2001): Permutation Methods: A Distance Function Approach. Springer-Verlag, New York, 352pp.

Spillane, M.C. (2009): Development of a Tsunami Forecast Model for Portland, Maine. NOAA OAR Special Report, PMEL Tsunami Forecast Series: Vol. NNNN, MMMM pp. (in progress).

Synolakis, C.E., E.N. Bernard, V.V. Titov, U. Kânoğlu, and F.I. González (2008): Validation and verification of tsunami numerical models. Pure Appl. Geophys., 165(11–12), 2197–2228.

Tang, L., V.V. Titov, Y. Wei, H.O. Mofjeld, M. Spillane, D. Arcas, E.N. Bernard, C. Chamberlin, E. Gica, and J. Newman (2008): Tsunami forecast analysis for the May 2006 Tonga tsunami. J. Geophys. Res., 113, C12015, doi: 10.1029/2008JC004922.

Tang, L., V. V. Titov, and C. D. Chamberlin (2009): Development, testing, and applications of site-specific tsunami inundation models for real-time forecasting, J. Geophys. Res., 114, C12025, doi:10.1029/2009JC005476.

Titov, V., and F.I. González (1997): Implementation and testing of the Method of Splitting Tsunami (MOST) model. NOAA Tech. Memo. ERL PMEL-112 (PB98-122773), NOAA/Pacific Marine Environmental Laboratory, Seattle, WA, 11 pp.

Titov, V.V., F.I. González, E.N. Bernard, M.C. Eble, H.O. Mofjeld, J.C. Newman, and A.J. Venturato (2005): Real-time tsunami forecasting: Challenges and solutions. Nat. Hazards, 35(1), Special Issue, U.S. National Tsunami Hazard Mitigation Program, 41–58.

Titov, V.V. (2009): Tsunami forecasting. Chapter 12 in The Sea, Volume 15: Tsunamis, Harvard University Press, Cambridge, MA and London, England, 371–400.

Watterson, I.G. (1996): Non-dimensional measures of climate model performance. Int. J. Climatol., 16, 379–391.

Wei, Y., E. Bernard, L. Tang, R. Weiss, V. Titov, C. Moore, M. Spillane, M. Hopkins, and U. Kânoğlu (2008): Real-time experimental forecast of the Peruvian tsunami of August 2007 for U.S. coastlines. Geophys. Res. Lett., 35, L04609, doi: 10.1029/2007GL032250.

Wei, Y. (2010): Development Of A Tsunami Forecast Model For Ocean City, Maryland. NOAA OAR Special Report, PMEL Tsunami Forecast Series: Vol. NNNN, MMMM pp. (in progress).

Willmott, CJ. (1981): On the validation of models. Phys. Geogr., 2, 184–194.

Willmott, C.J., Ackleson, S.G., Davis, R.E., Feddema, J.J., Klink K.M., Legates, D.R., O'Donnell, J. and Rowe, C.M. (1985): Statistics for the evaluation of model performance. J. Geophys. Res., 90(C5), 8995–9005.

Table 1: Tidal characteristics for the Bar Harbor tide gauge.

<table>
<tr><th>Bar Harbor, ME</th><th>Station ID:
8413320/ATGM1</th><th colspan="2">43° 23' 30"N, 68° 12' 18"W
44.3917°N, 68.2050°W</th></tr>
<tr><th colspan="4">Tidal Datum and Range Values (Epoch 1983 – 2001)</th></tr>
<tr><td>Mean Higher-High Water</td><td>4.524 m</td><td rowspan="4">Diurnal Range
3.466 m</td><td></td></tr>
<tr><td>Mean High Water</td><td>4.394 m</td><td rowspan="3">Mean Range
3.220 m</td></tr>
<tr><td>Mean Sea Level</td><td>2.786 m</td></tr>
<tr><td>Mean Low Water</td><td>1.174 m</td></tr>
<tr><td>Mean Lower-Low water</td><td>1.058 m</td><td></td></tr>
<tr><th colspan="4">Nearest corresponding model grid nodes</th></tr>
<tr><th></th><th>Depth at node</th><th>Node coordinates</th><th>Node index</th></tr>
<tr><td>Forecast model</td><td>2.03 m</td><td>44.3916°N,
68.2050°W</td><td>(88,72)</td></tr>
<tr><td>Reference model</td><td>3.22 m</td><td>44.3917°N,
68.2050°W</td><td>(262,213)</td></tr>
</table>

Data taken from http://tidesandcurrents.noaa.gov/geo.shtml?location=8413320.

Table 2: MOST setup parameters for reference and forecast models for Bar Harbor, Maine.

		Reference Model				Forecast Model			
Grid	**Region**	**Coverage Lat. [°N] Lon. [°W]**	**Cell Size [”]**	**nx × ny**	**Time Step [sec]**	**Coverage Lat. [°N] Lon. [°W]**	**Cell Size [”]**	**nx × ny**	**Time Step [sec]**
A	Gulf of Maine	37.0 – 46.25 288.0 – 297.0	30	1081 × 1111	2	39.3583 – 45.167 289.267 – 294.617	30	643 × 698	6.0
B	Mt Desert Island and surrounds	43.9 – 44.63 291.31 – 292.2	3	1069 × 877	1	43.9525 – 44.53 291.4867 – 2921.9767	9 × 12	148 × 232	3.0
C	Bar Harbor/ Frenchman Bay	44.33507 – 44.431 291.7467 – 291.8500	⅔	559 × 517	0.25	44.3354 – 44.431 291.7467 – 291.85	2	186 × 173	1
Minimum offshore depth [m]:			5			5			
Water depth for dry land [m]:			0.1			0.1			
Friction coefficient [n^2]:			0.009			0.009			
CPU time for 4-hr simulation:			269 min			21 min			

Computations were performed on a single core of a Dell PowerEdge R510 containing dual Intel Xeon hex-core X5670 processors running at 2.93 GHz.

Table 3: Synthetic tsunami events. The location of sources 1-5 and 7 are shown in Figure 8.

Source. Number	Source Zone	Tsunami Database Unit Source(s)	Scale factor	Equivalent M_W
Micro	South Sandwich	B11	0.05	7.3
1	Atlantic	A38-A47, B38-B47	25	9.3
2	Atlantic	A48-A57, B48-B57	25	9.3
3	Atlantic	A58-A67, B58-B67	25	9.3
4	Atlantic	A68-A77, B68-B77	25	9.3
5	Atlantic	A82-A91, B82-B91	25	9.3
6	South Sandwich	A1-A10, B1-B10	25	9.3
7	Atlantic	B52	1	7.5

Table 4: Values of various indices for each of the seven synthetic scenarios considered and the micro synthetic scenario. A description of the indices is given in Appendix C.

Scenario Number	ε_{max}	r	nRMSE	IOA	M	$\Re$
micro	-0.412	0.635	0.773	0.562	0.401	0.403
1	-0.291	0.703	0.711	0.582	0.459	0.439
2	-0.368	0.723	0.692	0.642	0.494	0.542
3	-0.307	0.853	0.522	0.727	0.639	0.621
4	-0.090	0.992	0.146	0.930	0.903	0.905
5	-0.351	0.970	0.301	0.846	0.787	0.771
6	-0.377	0.753	0.665	0.637	0.487	0.506
7	-0.418	0.369	0.940	0.367	0.195	0.167

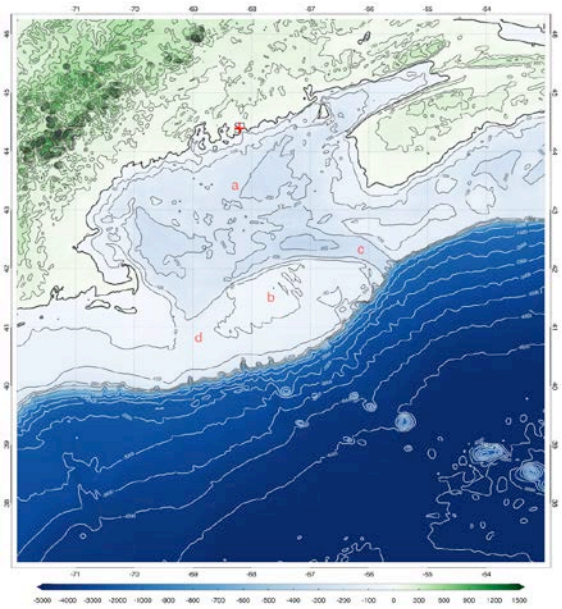

Figure 1: Contour relief of the Gulf of Maine. The features labeled are (a) the Gulf of Maine, (b) The Georges Bank (c) The Northeast Channel and (d) The Great South Channel. These features are referenced in the text. The red cross indicates the approximate location of Bar Harbor. Depths are in meters.

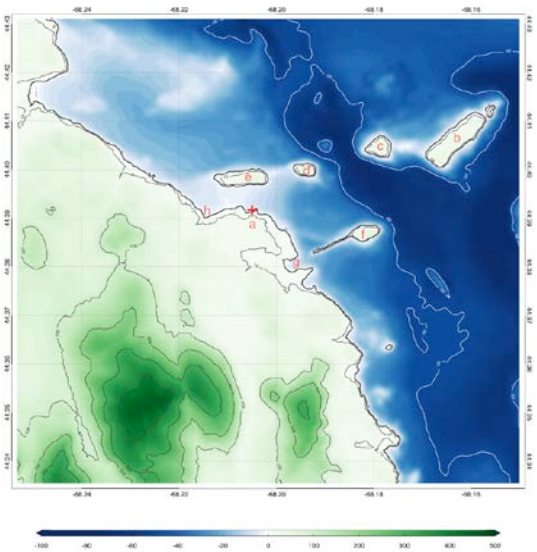

Figure 2: Contour relief of Frenchman bay. Units are in meters. The features labeled are (a) Bar Harbor township, (b) Long Porcupine Island, (c) Burnt Porcupine Island (d) Sheep Porcupine Island, (e) Bar Island, (f) Bald Porcupine Island (Note the breakwater extending east.), (g) Cromwell Cove (h) outflow region from Eddie Brook and (i) Hulls Cove. These features are referenced in the text. The red cross indicates the location of the tide gauge and depths are in meters.

Figure 3: Aerial photography of the Bar Harbor region. Key land features are labeled. Taken from Google Earth.

Figure 4: Oblique aerial view of the Bar Harbor region. Photograph by Flicker user Smudge 9000, used under Creative Commons Attribution 2.0.

Figure 5: Instrument housing for the Bar Harbor tide gauge.

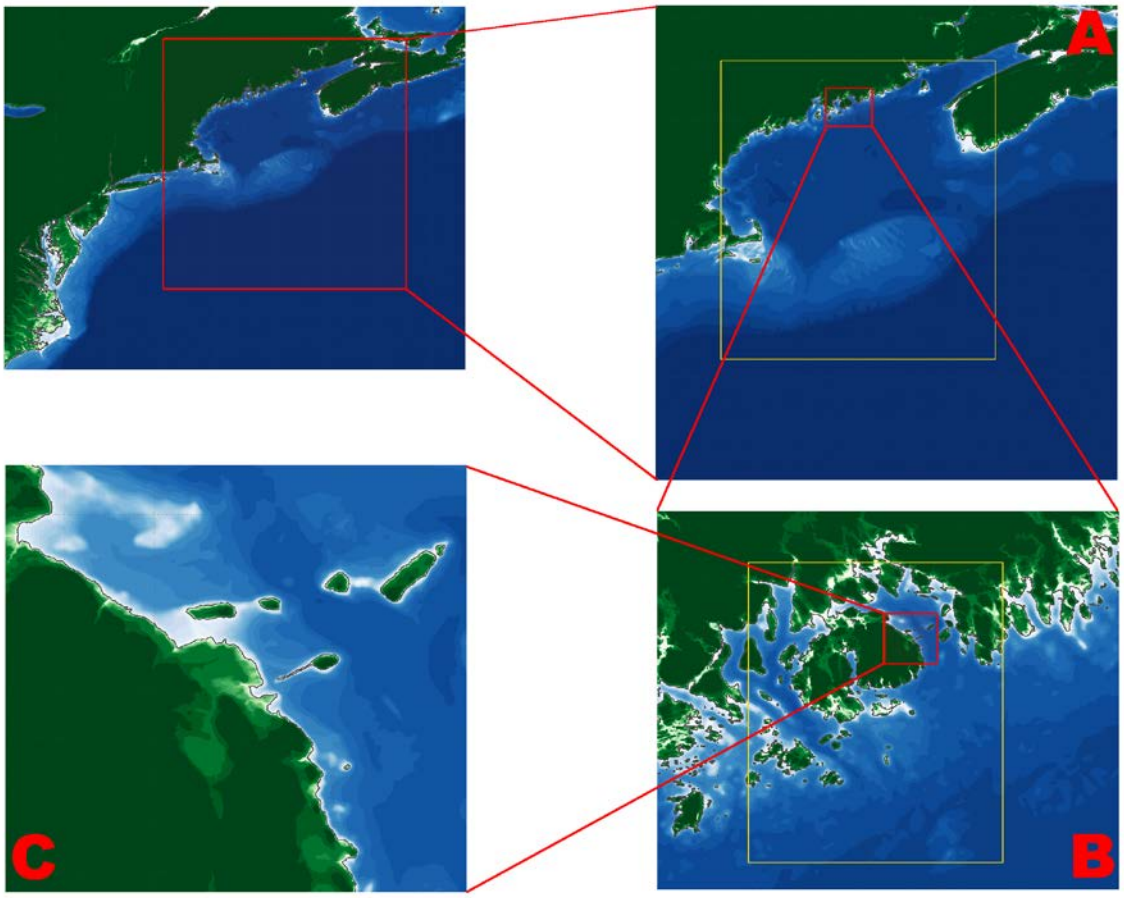

Figure 6: A depiction of the extent and location of the forecast grids, including how each is nested. The top-left figure shows the extent of the A reference grid. The top-right figure shows this grid in more detail with the extent of the A forecast grid shown by the yellow rectangle and the extent of the B reference grid shown by the red rectangle. The other figures follow in a similar manner. Note that there is no yellow rectangle depicting the extent of the C forecast grid, since it covers the same areas as the C reference grid.

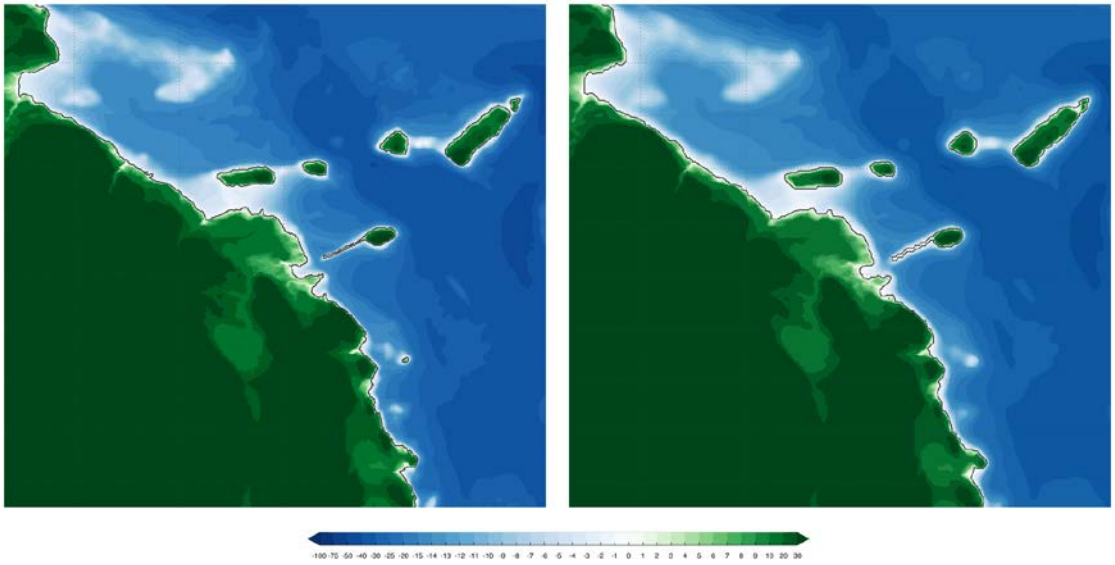

Figure 7: Comparison of the C reference grid (left) with the C forecast grid. Depths are in meters.

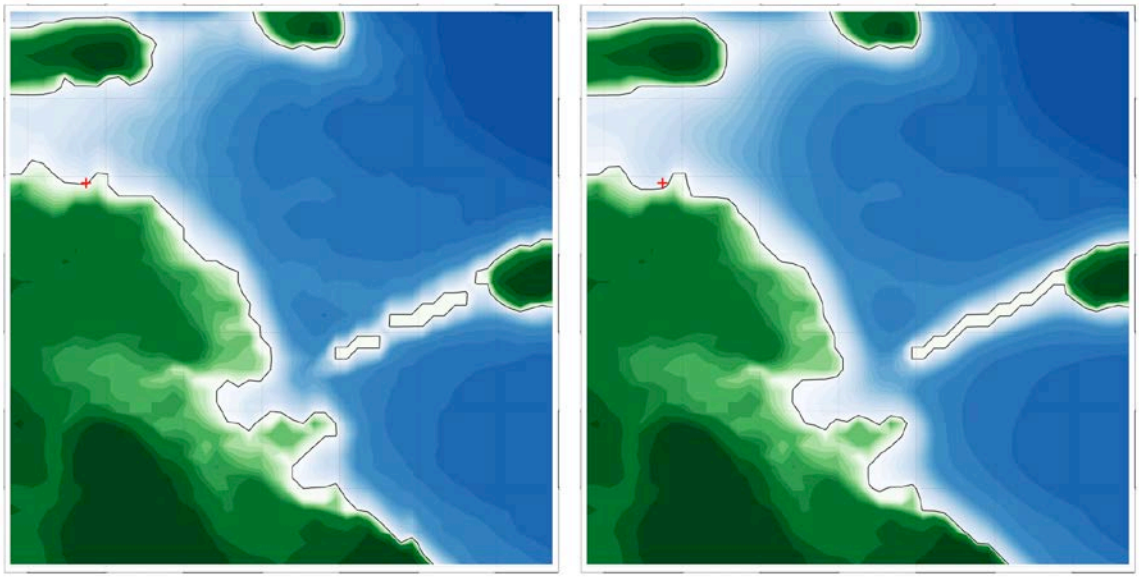

Figure 8: An example of some of the effects of necessary bathy modifications on the C forecast grid in the vicinity of Bar Harbor (the unmodified bathymetry is shown on the left). Note the changes to the breakwater and the area near the tide gauge (marked by the red cross). The effects of smoothing over the entire grid are also apparent on the form of the (underwater) contours.

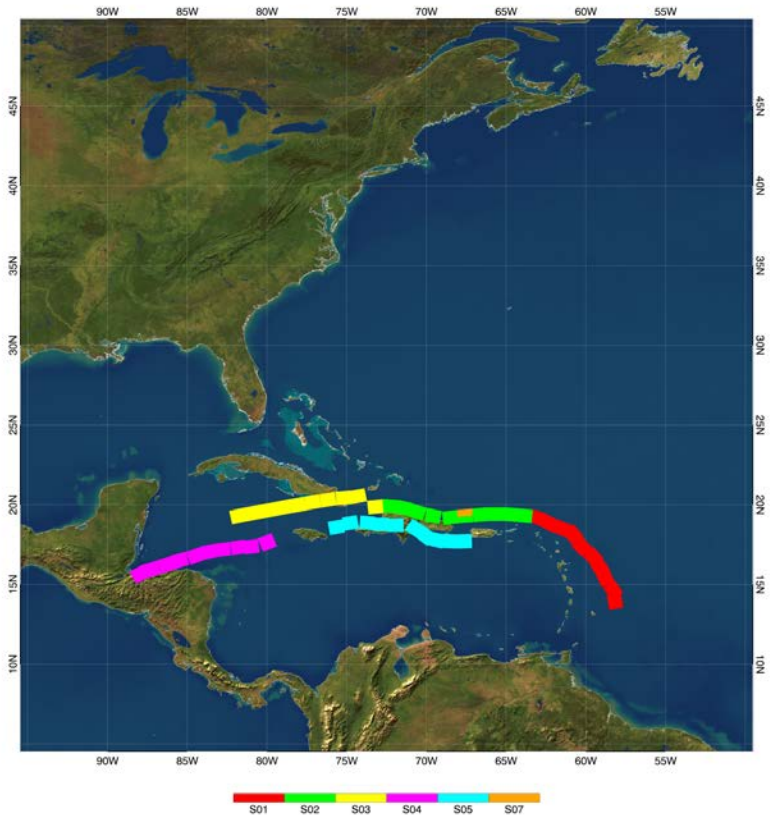

Figure 9: Location of Caribbean unit sources. The synthetic scenarios used in this study consist of scaling and combining these unit sources. The unit sources that make up each scenario are colored according to the key. The single unit source that comprises scenario 7 is also used by scenario 2.

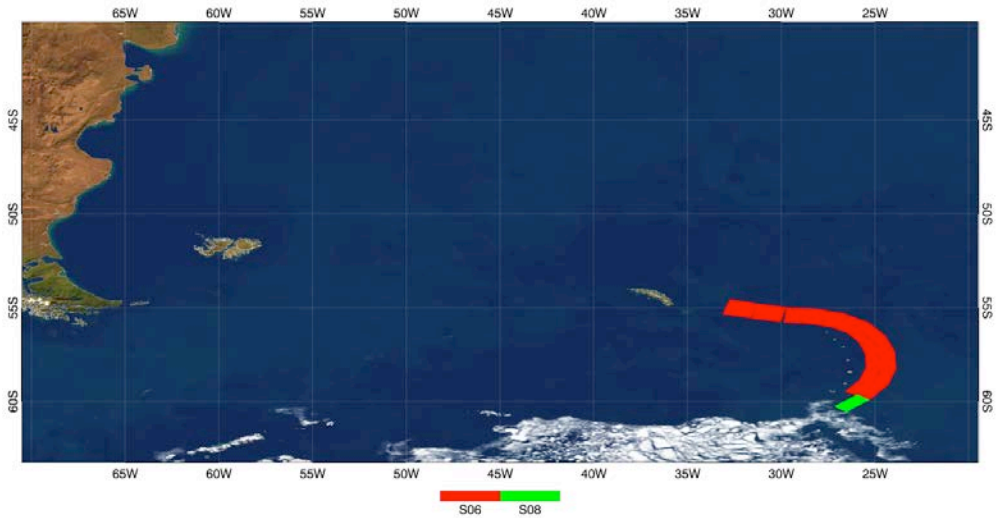

Figure 10: Location of the South Sandwich Sources. As in Figure 9, the unit sources that make up each scenario are colored according to the key.

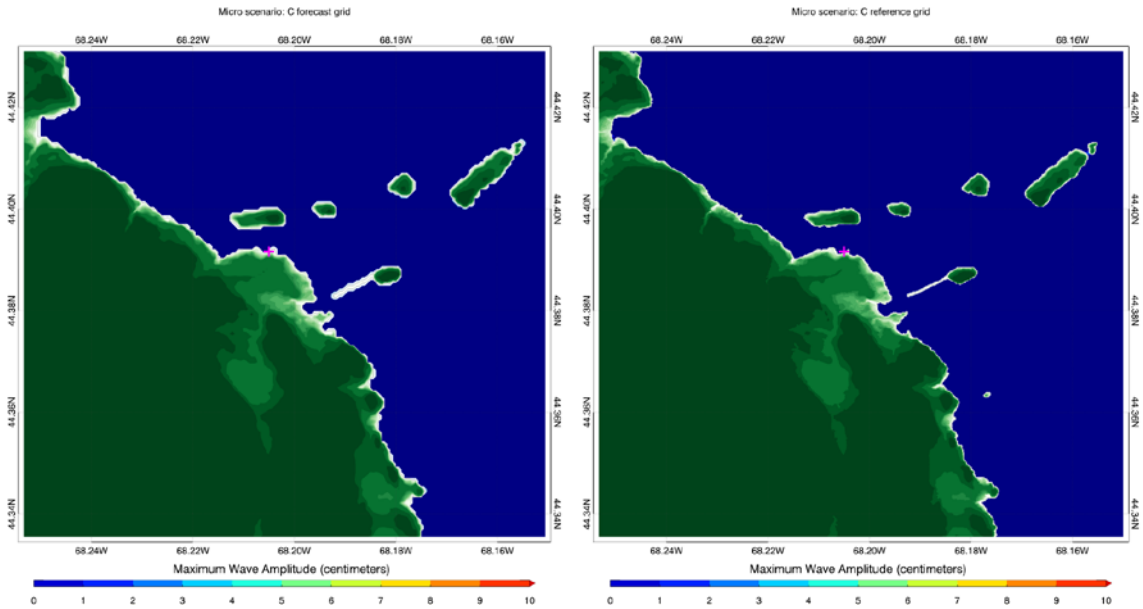

Figure 11: Plot of maximum amplitude for both the forecast and reference C grids for the micro scenario. Units are in cm and the magenta cross shows the location of the tide gauge.

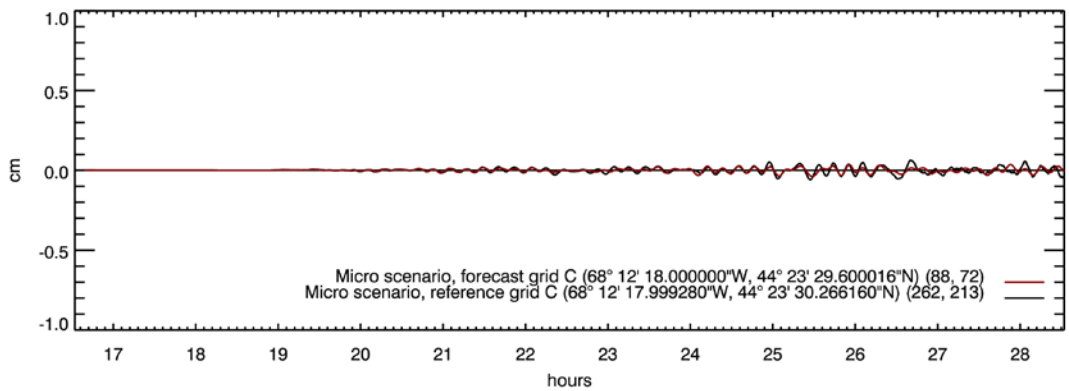

Figure 12: Time series of sea-level elevations at the forecast and reference grid nodes nearest the Bar Harbor tide gauge for the micro scenario. The series from the forecast grid is shown in in red and the series for the reference model is shown in black. Units are in cm. The length of both series is 12 hours, calculated from when the tsunami first reaches the edge of the respective A grids.

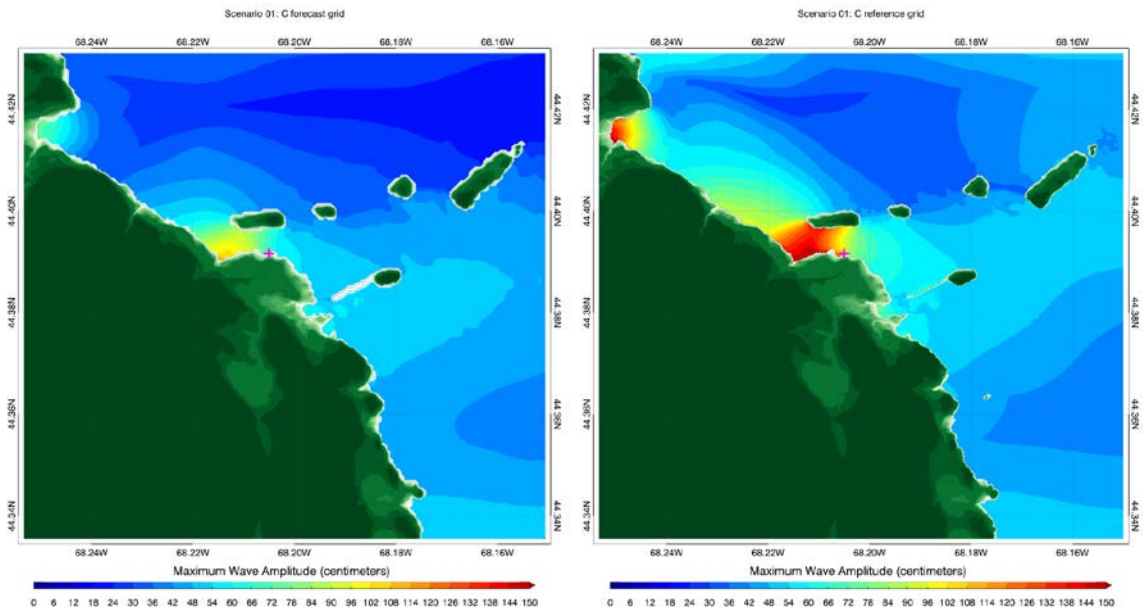

Figure 13: Plot of maximum amplitude for both the forecast and reference C grids for the scenario 1. Units are in cm and the magenta cross shows the location of the tide gauge.

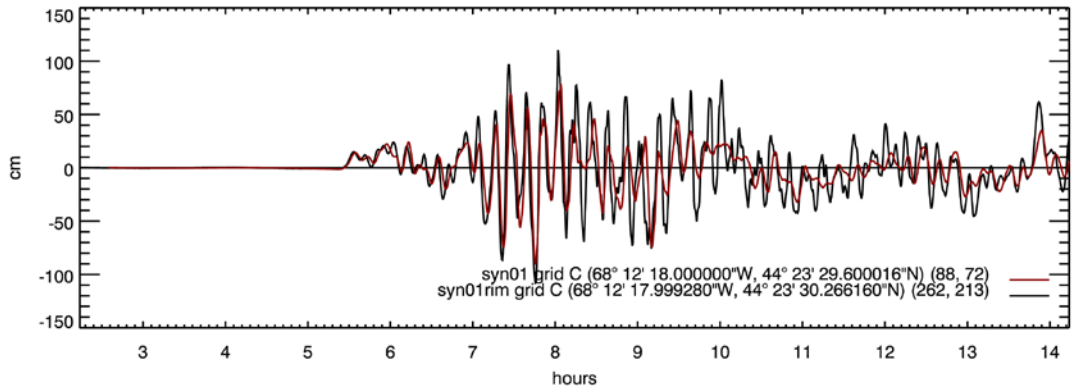

Figure 14: Time series of sea-level elevations at the forecast and reference grid nodes nearest the Bar Harbor tide gauge for scenario 1. The series from the forecast grid is shown in in red and the series for the reference model is shown in black. Units are in cm.

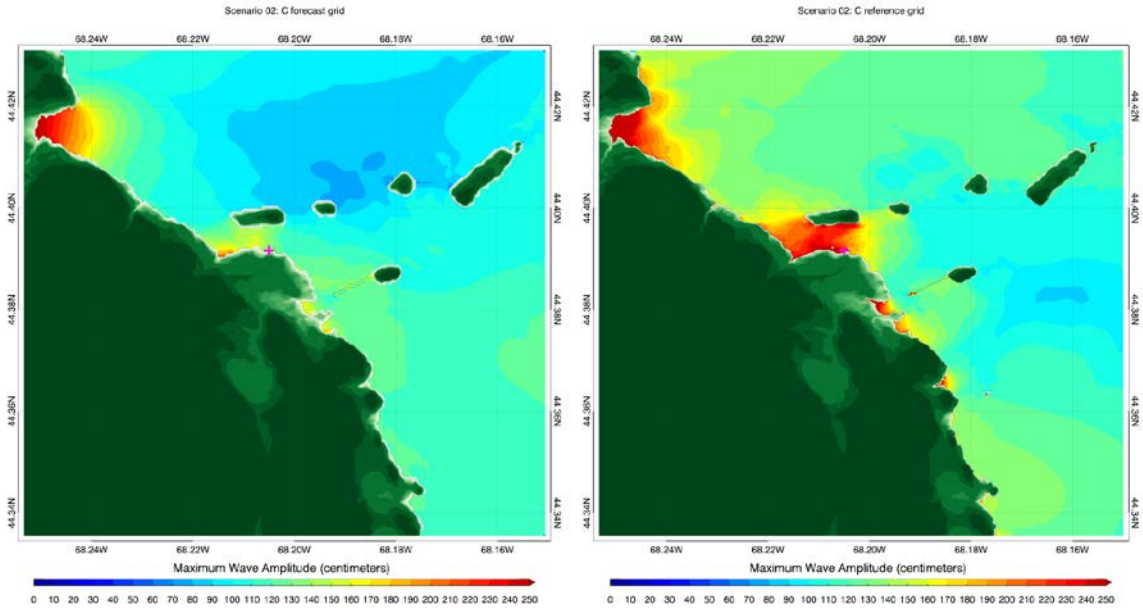

Figure 15: Plot of maximum amplitude for both the forecast and reference C grids for the scenario 2. Units are in cm and the magenta cross shows the location of the tide gauge.

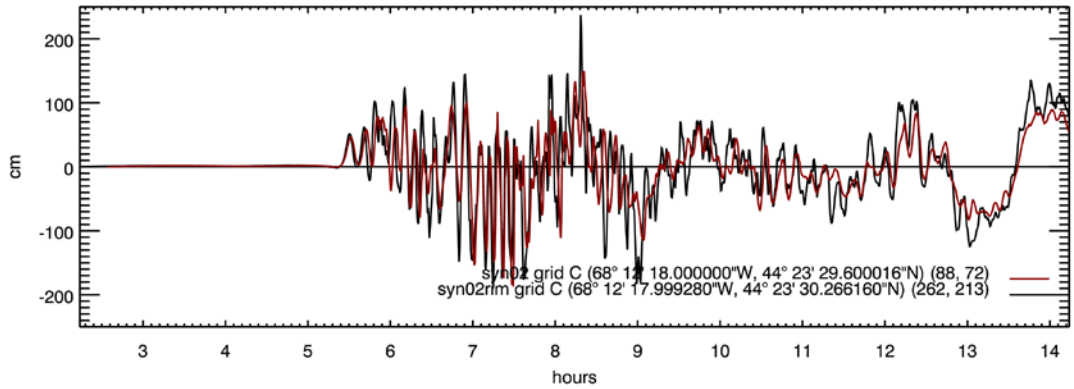

Figure 16: Time series of sea-level elevations at the forecast and reference grid nodes nearest the Bar Harbor tide gauge for scenario 2. The series from the forecast grid is shown in in red and the series for the reference model is shown in black. Units are in cm.

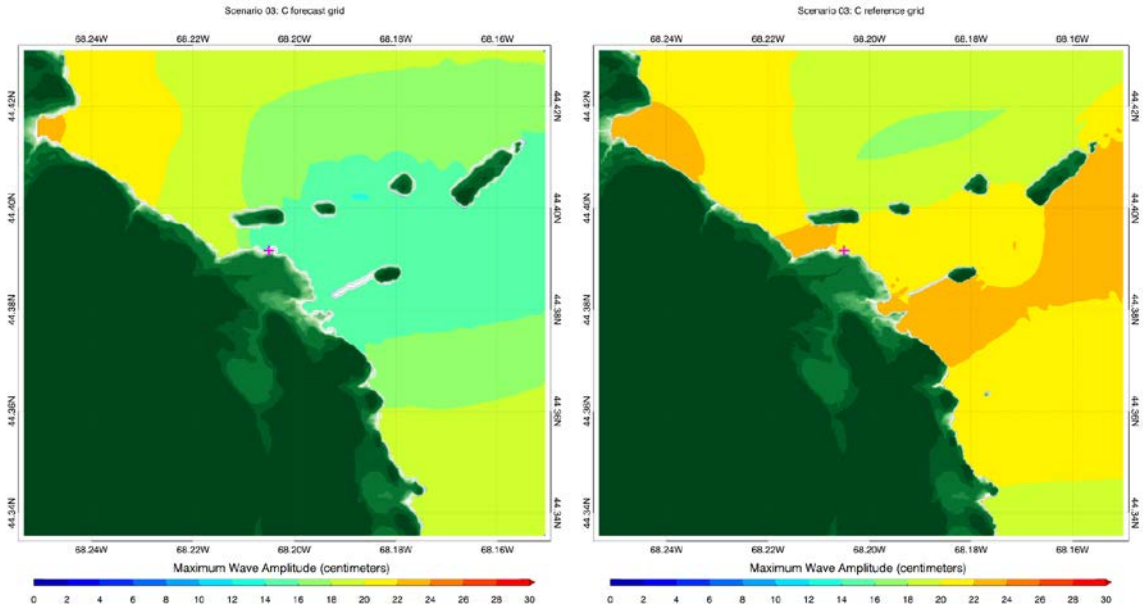

Figure 17: Plot of maximum amplitude for both the forecast and reference C grids for the scenario 3. Units are in cm and the magenta cross shows the location of the tide gauge.

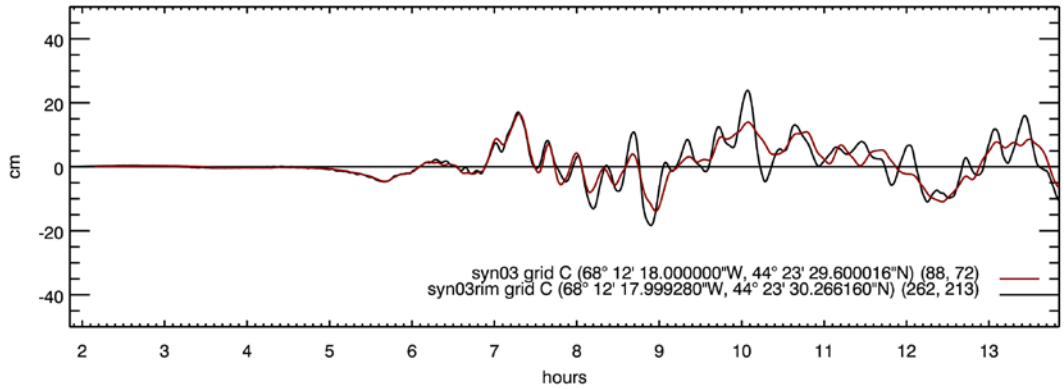

Figure 18: Time series of sea-level elevations at the forecast and reference grid nodes nearest the Bar Harbor tide gauge for scenario 3. The series from the forecast grid is shown in in red and the series for the reference model is shown in black. Units are in cm.

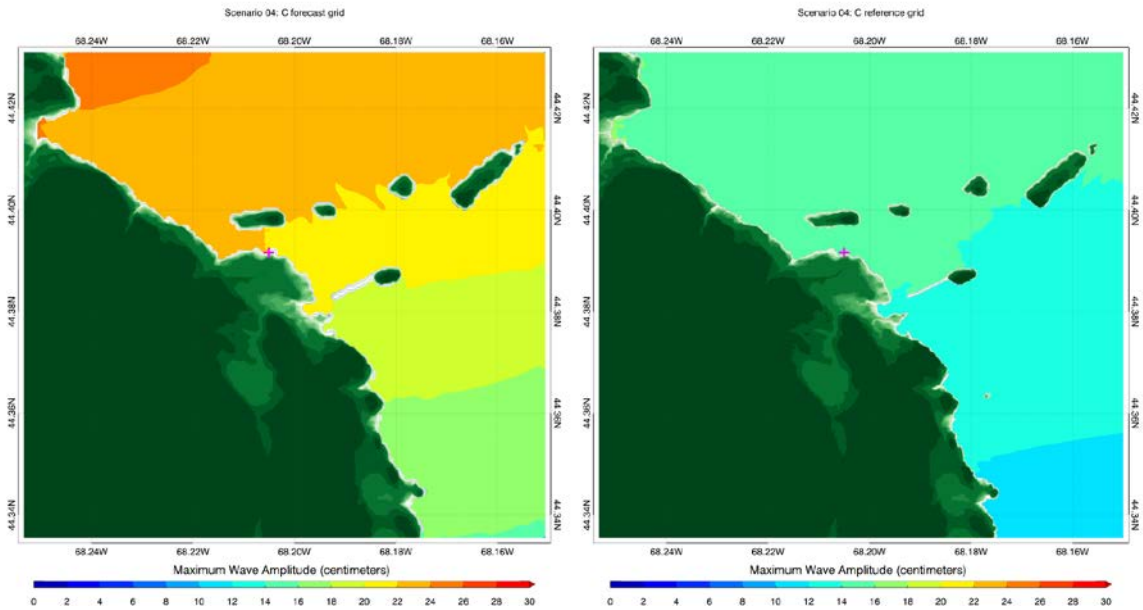

Figure 19: Plot of maximum amplitude for both the forecast and reference C grids for the scenario 4. Units are in cm and the magenta cross shows the location of the tide gauge.

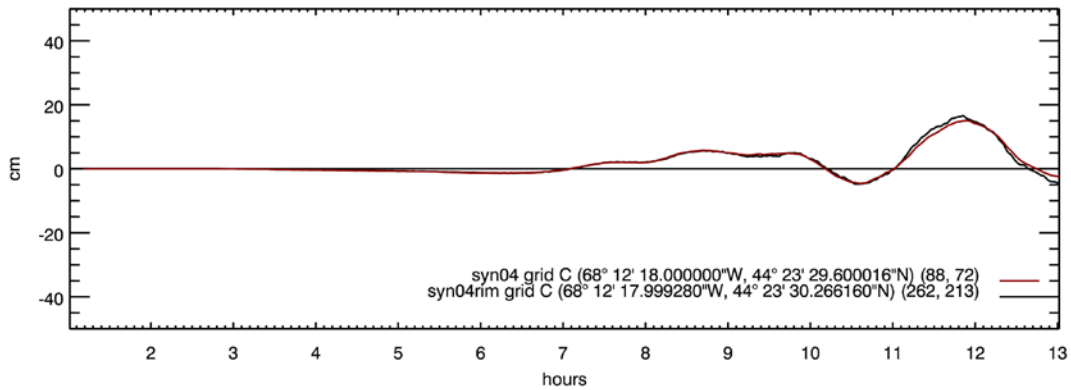

Figure 20: Time series of sea-level elevations at the forecast and reference grid nodes nearest the Bar Harbor tide gauge for scenario 4. The series from the forecast grid is shown in in red and the series for the reference model is shown in black. Units are in cm.

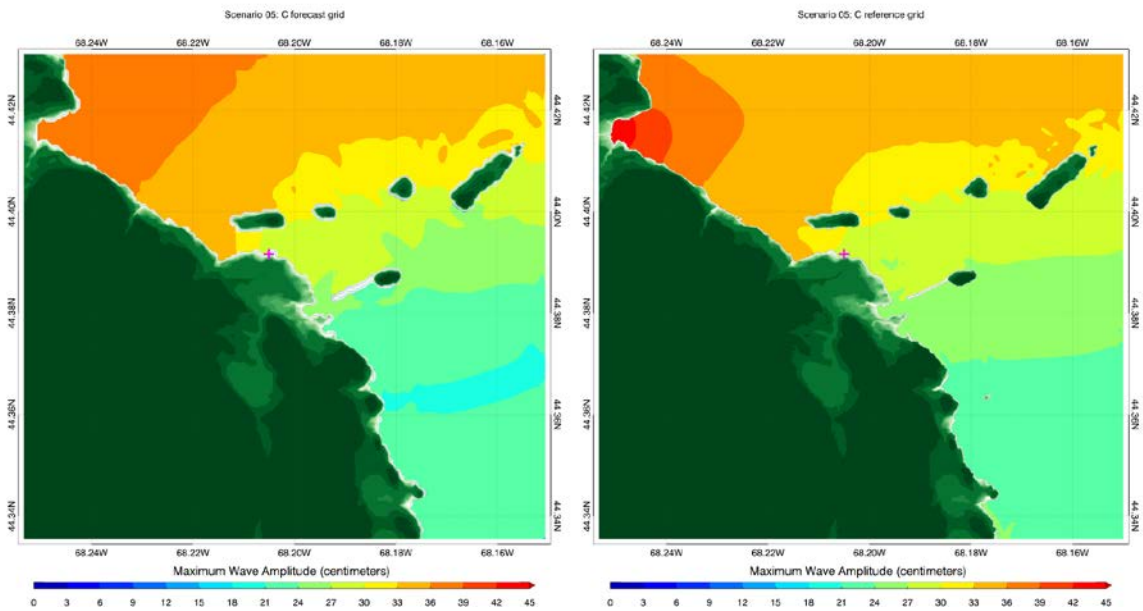

Figure 21: Plot of maximum amplitude for both the forecast and reference C grids for the scenario 5. Units are in cm and the magenta cross shows the location of the tide gauge.

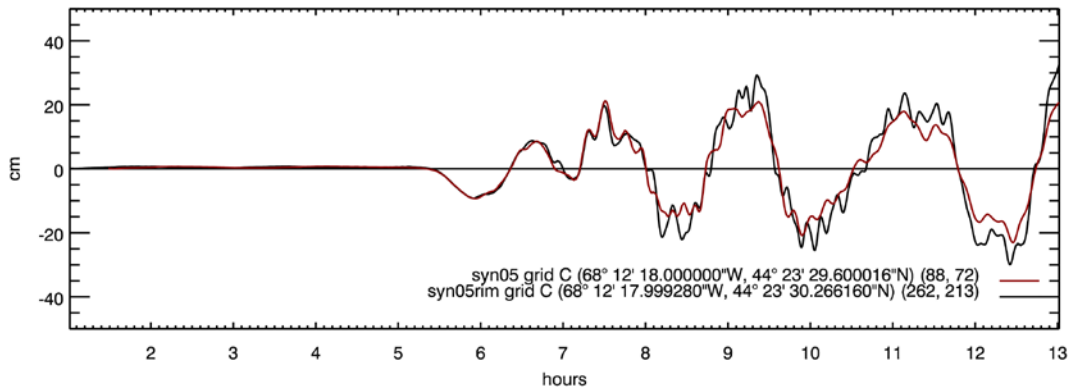

Figure 22: Time series of sea-level elevations at the forecast and reference grid nodes nearest the Bar Harbor tide gauge for scenario 5. The series from the forecast grid is shown in in red and the series for the reference model is shown in black. Units are in cm.

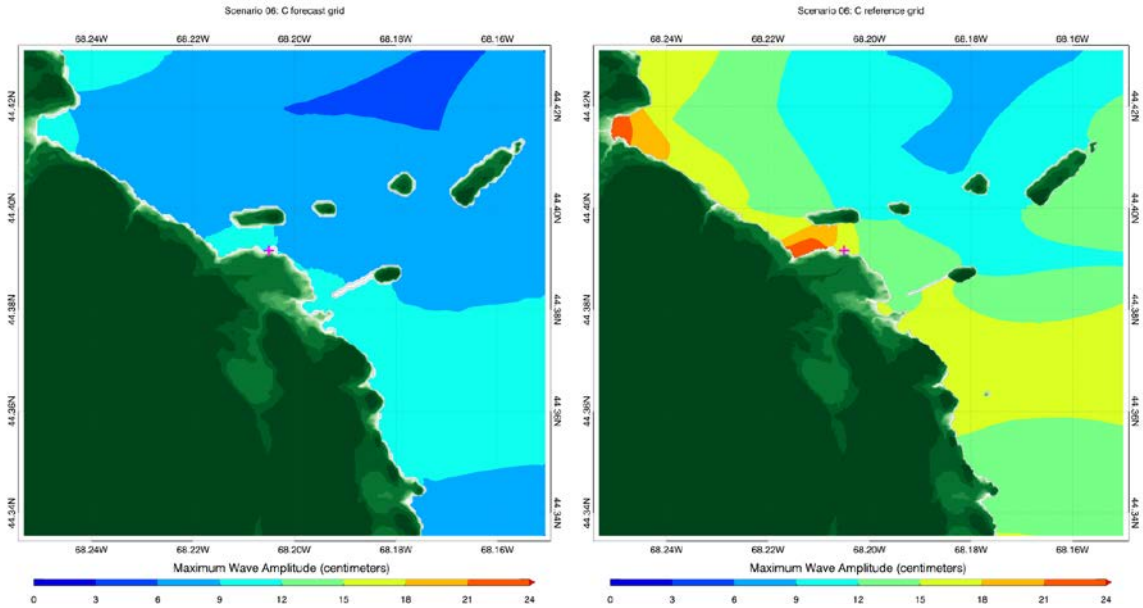

Figure 23: Plot of maximum amplitude for both the forecast and reference C grids for the scenario 6. Units are in cm and the magenta cross shows the location of the tide gauge.

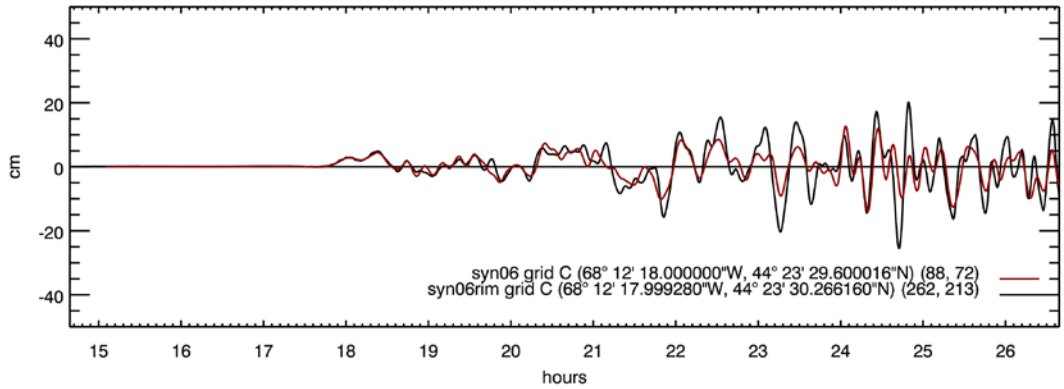

Figure 24: Time series of sea-level elevations at the forecast and reference grid nodes nearest the Bar Harbor tide gauge for scenario 6. The series from the forecast grid is shown in in red and the series for the reference model is shown in black. Units are in cm.

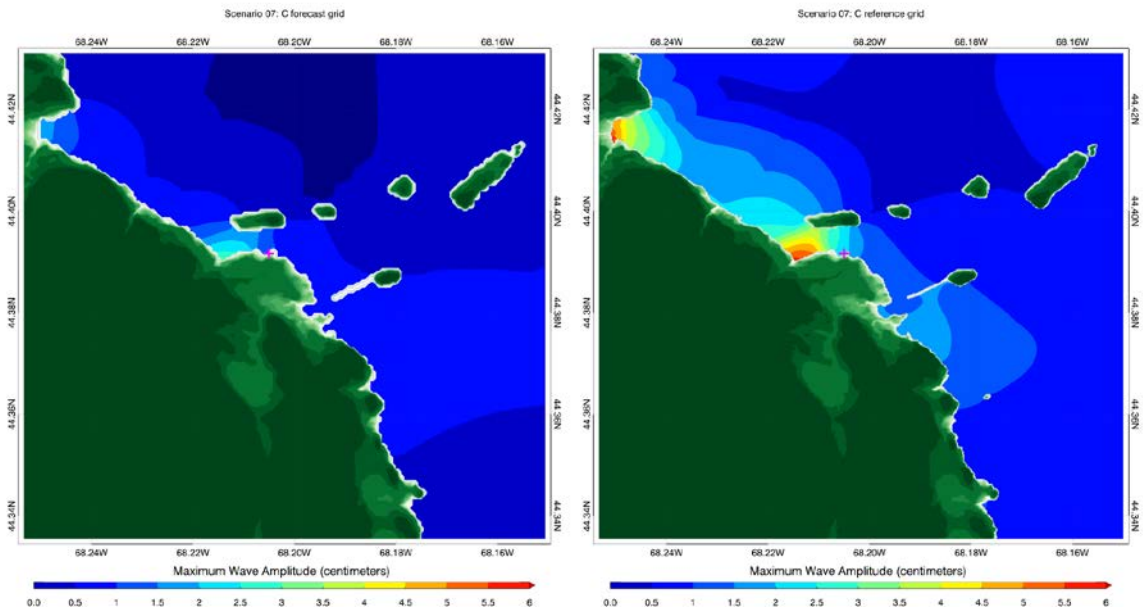

Figure 25: Plot of maximum amplitude for both the forecast and reference C grids for the scenario 7. Units are in cm and the magenta cross shows the location of the tide gauge.

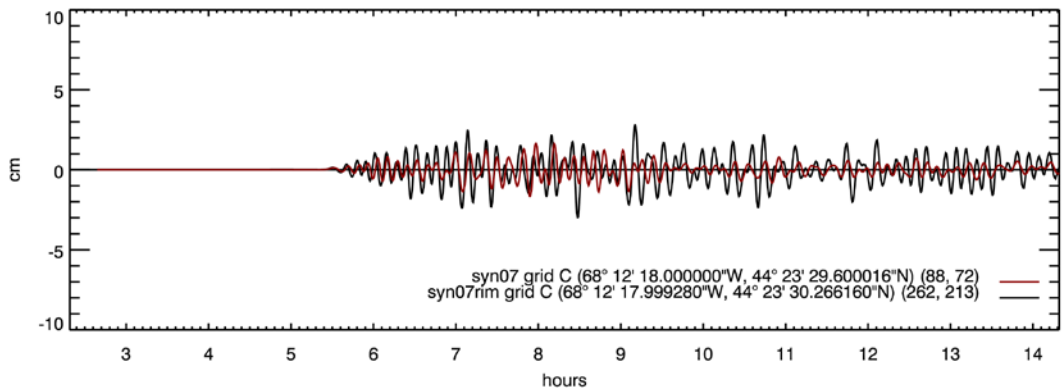

Figure 26: Time series of sea-level elevations at the forecast and reference grid nodes nearest the Bar Harbor tide gauge for scenario 7. The series from the forecast grid is shown in in red and the series for the reference model is shown in black. Units are in cm.

Appendix A

Development of the Bar Harbor, Maine tsunami forecast model occurred prior to parameter changes that were made to reflect modifications to the MOST model code. As a result, the input file for running both the optimized tsunami forecast model and the high-resolution reference inundation model in MOST have been updated accordingly. Appendix A1 and A2 provide the updated files for Bar Harbor, Maine.

A.1 Reference model *.in file

```
0.0001      Minimum amplitude of input offshore wave (m)
5.0     Input minimum depth for offshore (m)
0.1     Input "dry land" depth for inundation (m)
0.0009      Input friction coefficient (n**2)
1       A & B-grid runup flag (0=disallow, 1=allow runup)
100.0   Blow-up limit (maximum eta before blow-up)
0.25    Input time step (sec)
172800      Input number of steps
8       Compute "A" arrays every nth time step, n=
4       Compute "B" arrays every nth time step, n=
120     Input number of steps between snapshots
1       ...Starting from
1       ...Saving grid every nth node, n=1
```

A.2 Forecast Model *.in file

```
0.0001      Minimum amplitude of input offshore wave (m)
5.0     Input minimum depth for offshore (m)
0.1     Input "dry land" depth for inundation (m)
0.0009      Input friction coefficient (n**2)
1       A & B-grid runup flag (0=disallow, 1=allow runup)
100.0   Blow-up limit (maximum eta before blow-up)
1.0     Input time step (sec)
43200       Input number of steps
3       Compute "A" arrays every nth time step, n=
6       Compute "B" arrays every nth time step, n=
30      Input number of steps between snapshots
1       ...Starting from
1       ...Saving grid every nth node, n=1
```

Appendix B. Propagation Database: Atlantic Ocean Unit Sources.

Propagation source details reflect the database as of January 29, 2013. The development of Bar Harbor, Maine forecast inundation model uses the propagation database as of 2012 thus there is a possibility of changes due to updates in the earthquake source parameters after this date.

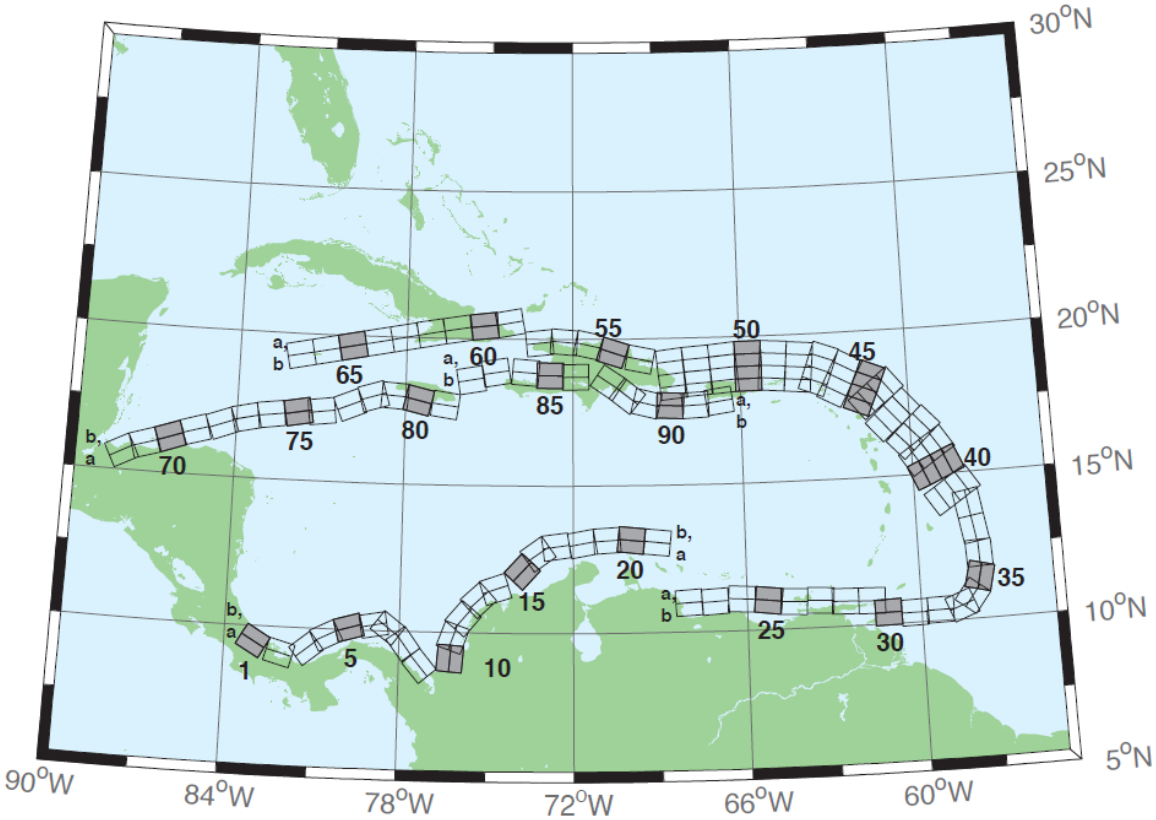

Figure 27. Atlantic Source unit sources

Table 5. Earthquake parameters for Atlantic Source Zone unit sources.

Segment	Description	Longitude (°E)	Latitude (°)	Strike (°)	Dip (°)	Depth (km)
atsz-01_a	Atlantic Source Zone	-83.2020	9.1449	27.50	120.00	28.09
atsz-01_b	Atlantic Source Zone	-83.0000	9.4899	27.50	120.00	5.00
atsz-02_a	Atlantic Source Zone	-82.1932	8.7408	27.50	105.11	28.09
atsz-02_b	Atlantic Source Zone	-82.0880	9.1254	27.50	105.11	5.00
atsz-03_a	Atlantic Source Zone	-80.9172	9.0103	30.00	51.31	30.00
atsz-03_b	Atlantic Source Zone	-81.1636	9.3139	30.00	51.31	5.00
atsz-04_a	Atlantic Source Zone	-80.3265	9.4308	30.00	63.49	30.00
atsz-04_b	Atlantic Source Zone	-80.5027	9.7789	30.00	63.49	5.00
atsz-05_a	Atlantic Source Zone	-79.6247	9.6961	30.00	74.44	30.00
atsz-05_b	Atlantic Source Zone	-79.7307	10.0708	30.00	74.44	5.00
atsz-06_a	Atlantic Source Zone	-78.8069	9.8083	30.00	79.71	30.00
atsz-06_b	Atlantic Source Zone	-78.8775	10.1910	30.00	79.71	5.00
atsz-07_a	Atlantic Source Zone	-78.6237	9.7963	30.00	127.25	30.00
atsz-07_b	Atlantic Source Zone	-78.3845	10.1059	30.00	127.25	5.00
atsz-08_a	Atlantic Source Zone	-78.1693	9.3544	30.00	143.76	30.00
atsz-08_b	Atlantic Source Zone	-77.8511	9.5844	30.00	143.76	5.00
atsz-09_a	Atlantic Source Zone	-77.5913	8.5989	30.00	139.93	30.00
atsz-09_b	Atlantic Source Zone	-77.2900	8.8493	30.00	139.93	5.00
atsz-10_a	Atlantic Source Zone	-75.8109	9.0881	17.00	4.67	19.62
atsz-10_b	Atlantic Source Zone	-76.2445	9.1231	17.00	4.67	5.00
atsz-11_a	Atlantic Source Zone	-75.7406	9.6929	17.00	19.67	19.62
atsz-11_b	Atlantic Source Zone	-76.1511	9.8375	17.00	19.67	5.00
atsz-12_a	Atlantic Source Zone	-75.4763	10.2042	17.00	40.40	19.62
atsz-12_b	Atlantic Source Zone	-75.8089	10.4826	17.00	40.40	5.00
atsz-13_a	Atlantic Source Zone	-74.9914	10.7914	17.00	47.17	19.62
atsz-13_b	Atlantic Source Zone	-75.2890	11.1064	17.00	47.17	5.00
atsz-14_a	Atlantic Source Zone	-74.5666	11.0708	17.00	71.68	19.62
atsz-14_b	Atlantic Source Zone	-74.7043	11.4786	17.00	71.68	5.00
atsz-15_a	Atlantic Source Zone	-73.4576	11.8012	17.00	42.69	19.62
atsz-15_b	Atlantic Source Zone	-73.7805	12.0924	17.00	42.69	5.00
atsz-16_a	Atlantic Source Zone	-72.9788	12.3365	17.00	54.75	19.62
atsz-16_b	Atlantic Source Zone	-73.2329	12.6873	17.00	54.75	5.00
atsz-17_a	Atlantic Source Zone	-72.5454	12.5061	17.00	81.96	19.62
atsz-17_b	Atlantic Source Zone	-72.6071	12.9314	17.00	81.96	5.00
atsz-18_a	Atlantic Source Zone	-71.6045	12.6174	17.00	79.63	19.62
atsz-18_b	Atlantic Source Zone	-71.6839	13.0399	17.00	79.63	5.00
atsz-19_a	Atlantic Source Zone	-70.7970	12.7078	17.00	86.32	19.62
atsz-19_b	Atlantic Source Zone	-70.8253	13.1364	17.00	86.32	5.00
atsz-20_a	Atlantic Source Zone	-70.0246	12.7185	17.00	95.94	19.62

Table 5. continued

Segment	Description	Longitude (°E)	Latitude (°)	Strike (°)	Dip (°)	Depth (km)
atsz-20_b	Atlantic Source Zone	-69.9789	13.1457	17.00	95.94	5.00
atsz-21_a	Atlantic Source Zone	-69.1244	12.6320	17.00	95.94	19.62
atsz-21_b	Atlantic Source Zone	-69.0788	13.0592	17.00	95.94	5.00
atsz-22_a	Atlantic Source Zone	-68.0338	11.4286	15.00	266.94	17.94
atsz-22_b	Atlantic Source Zone	-68.0102	10.9954	15.00	266.94	5.00
atsz-23_a	Atlantic Source Zone	-67.1246	11.4487	15.00	266.94	17.94
atsz-23_b	Atlantic Source Zone	-67.1010	11.0155	15.00	266.94	5.00
atsz-24_a	Atlantic Source Zone	-66.1656	11.5055	15.00	273.30	17.94
atsz-24_b	Atlantic Source Zone	-66.1911	11.0724	15.00	273.30	5.00
atsz-25_a	Atlantic Source Zone	-65.2126	11.4246	15.00	276.36	17.94
atsz-25_b	Atlantic Source Zone	-65.2616	10.9934	15.00	276.36	5.00
atsz-26_a	Atlantic Source Zone	-64.3641	11.3516	15.00	272.87	17.94
atsz-26_b	Atlantic Source Zone	-64.3862	10.9183	15.00	272.87	5.00
atsz-27_a	Atlantic Source Zone	-63.4472	11.3516	15.00	272.93	17.94
atsz-27_b	Atlantic Source Zone	-63.4698	10.9183	15.00	272.93	5.00
atsz-28_a	Atlantic Source Zone	-62.6104	11.2831	15.00	271.11	17.94
atsz-28_b	Atlantic Source Zone	-62.6189	10.8493	15.00	271.11	5.00
atsz-29_a	Atlantic Source Zone	-61.6826	11.2518	15.00	271.57	17.94
atsz-29_b	Atlantic Source Zone	-61.6947	10.8181	15.00	271.57	5.00
atsz-30_a	Atlantic Source Zone	-61.1569	10.8303	15.00	269.01	17.94
atsz-30_b	Atlantic Source Zone	-61.1493	10.3965	15.00	269.01	5.00
atsz-31_a	Atlantic Source Zone	-60.2529	10.7739	15.00	269.01	17.94
atsz-31_b	Atlantic Source Zone	-60.2453	10.3401	15.00	269.01	5.00
atsz-32_a	Atlantic Source Zone	-59.3510	10.8123	15.00	269.01	17.94
atsz-32_b	Atlantic Source Zone	-59.3734	10.3785	15.00	269.01	5.00
atsz-33_a	Atlantic Source Zone	-58.7592	10.8785	15.00	248.62	17.94
atsz-33_b	Atlantic Source Zone	-58.5984	10.4745	15.00	248.62	5.00
atsz-34_a	Atlantic Source Zone	-58.5699	11.0330	15.00	217.15	17.94
atsz-34_b	Atlantic Source Zone	-58.2179	10.7710	15.00	217.15	5.00
atsz-35_a	Atlantic Source Zone	-58.3549	11.5300	15.00	193.68	17.94
atsz-35_b	Atlantic Source Zone	-57.9248	11.4274	15.00	193.68	5.00
atsz-36_a	Atlantic Source Zone	-58.3432	12.1858	15.00	177.65	17.94
atsz-36_b	Atlantic Source Zone	-57.8997	12.2036	15.00	177.65	5.00
atsz-37_a	Atlantic Source Zone	-58.4490	12.9725	15.00	170.73	17.94
atsz-37_b	Atlantic Source Zone	-58.0095	13.0424	15.00	170.73	5.00
atsz-38_a	Atlantic Source Zone	-58.6079	13.8503	15.00	170.22	17.94
atsz-38_b	Atlantic Source Zone	-58.1674	13.9240	15.00	170.22	5.00
atsz-39_a	Atlantic Source Zone	-58.6667	14.3915	15.00	146.85	17.94
atsz-39_b	Atlantic Source Zone	-58.2913	14.6287	15.00	146.85	5.00
atsz-39_y	Atlantic Source Zone	-59.4168	13.9171	15.00	146.85	43.82

Table 5. continued.

Segment	Description	Longitude (°E)	Latitude (°)	Strike (°)	Dip (°)	Depth (km)
atsz-39_z	Atlantic Source Zone	-59.0415	14.1543	15.00	146.85	30.88
atsz-40_a	Atlantic Source Zone	-59.1899	15.2143	15.00	156.23	17.94
atsz-40_b	Atlantic Source Zone	-58.7781	15.3892	15.00	156.23	5.00
atsz-40_y	Atlantic Source Zone	-60.0131	14.8646	15.00	156.23	43.82
atsz-40_z	Atlantic Source Zone	-59.6012	15.0395	15.00	156.23	30.88
atsz-41_a	Atlantic Source Zone	-59.4723	15.7987	15.00	146.33	17.94
atsz-41_b	Atlantic Source Zone	-59.0966	16.0392	15.00	146.33	5.00
atsz-41_y	Atlantic Source Zone	-60.2229	15.3177	15.00	146.33	43.82
atsz-41_z	Atlantic Source Zone	-59.8473	15.5582	15.00	146.33	30.88
atsz-42_a	Atlantic Source Zone	-59.9029	16.4535	15.00	136.99	17.94
atsz-42_b	Atlantic Source Zone	-59.5716	16.7494	15.00	136.99	5.00
atsz-42_y	Atlantic Source Zone	-60.5645	15.8616	15.00	136.99	43.82
atsz-42_z	Atlantic Source Zone	-60.2334	16.1575	15.00	136.99	30.88
atsz-43_a	Atlantic Source Zone	-60.5996	17.0903	15.00	138.71	17.94
atsz-43_b	Atlantic Source Zone	-60.2580	17.3766	15.00	138.71	5.00
atsz-43_y	Atlantic Source Zone	-61.2818	16.5177	15.00	138.71	43.82
atsz-43_z	Atlantic Source Zone	-60.9404	16.8040	15.00	138.71	30.88
atsz-44_a	Atlantic Source Zone	-61.1559	17.8560	15.00	141.07	17.94
atsz-44_b	Atlantic Source Zone	-60.8008	18.1286	15.00	141.07	5.00
atsz-44_y	Atlantic Source Zone	-61.8651	17.3108	15.00	141.07	43.82
atsz-44_z	Atlantic Source Zone	-61.5102	17.5834	15.00	141.07	30.88
atsz-45_a	Atlantic Source Zone	-61.5491	18.0566	15.00	112.84	17.94
atsz-45_b	Atlantic Source Zone	-61.3716	18.4564	15.00	112.84	5.00
atsz-45_y	Atlantic Source Zone	-61.9037	17.2569	15.00	112.84	43.82
atsz-45_z	Atlantic Source Zone	-61.7260	17.6567	15.00	112.84	30.88
atsz-46_a	Atlantic Source Zone	-62.4217	18.4149	15.00	117.86	17.94
atsz-46_b	Atlantic Source Zone	-62.2075	18.7985	15.00	117.86	5.00
atsz-46_y	Atlantic Source Zone	-62.8493	17.6477	15.00	117.86	43.82
atsz-46_z	Atlantic Source Zone	-62.6352	18.0313	15.00	117.86	30.88
atsz-47_a	Atlantic Source Zone	-63.1649	18.7844	20.00	110.46	22.10
atsz-47_b	Atlantic Source Zone	-63.0087	19.1798	20.00	110.46	5.00
atsz-47_y	Atlantic Source Zone	-63.4770	17.9936	20.00	110.46	56.30
atsz-47_z	Atlantic Source Zone	-63.3205	18.3890	20.00	110.46	39.20
atsz-48_a	Atlantic Source Zone	-63.8800	18.8870	20.00	95.37	22.10
atsz-48_b	Atlantic Source Zone	-63.8382	19.3072	20.00	95.37	5.00
atsz-48_y	Atlantic Source Zone	-63.9643	18.0465	20.00	95.37	56.30
atsz-48_z	Atlantic Source Zone	-63.9216	18.4667	20.00	95.37	39.20
atsz-49_a	Atlantic Source Zone	-64.8153	18.9650	20.00	94.34	22.10
atsz-49_b	Atlantic Source Zone	-64.7814	19.3859	20.00	94.34	5.00
atsz-49_y	Atlantic Source Zone	-64.8840	18.1233	20.00	94.34	56.30

Table 5. continued.

Segment	Description	Longitude (°E)	Latitude (°)	Strike (°)	Dip (°)	Depth (km)
atsz-49_z	Atlantic Source Zone	-64.8492	18.5442	20.00	94.34	39.20
atsz-50_a	Atlantic Source Zone	-65.6921	18.9848	20.00	89.59	22.10
atsz-50_b	Atlantic Source Zone	-65.6953	19.4069	20.00	89.59	5.00
atsz-50_y	Atlantic Source Zone	-65.6874	18.1407	20.00	89.59	56.30
atsz-50_z	Atlantic Source Zone	-65.6887	18.5628	20.00	89.59	39.20
atsz-51_a	Atlantic Source Zone	-66.5742	18.9484	20.00	84.98	22.10
atsz-51_b	Atlantic Source Zone	-66.6133	19.3688	20.00	84.98	5.00
atsz-51_y	Atlantic Source Zone	-66.4977	18.1076	20.00	84.98	56.30
atsz-51_z	Atlantic Source Zone	-66.5353	18.5280	20.00	84.98	39.20
atsz-52_a	Atlantic Source Zone	-67.5412	18.8738	20.00	85.87	22.10
atsz-52_b	Atlantic Source Zone	-67.5734	19.2948	20.00	85.87	5.00
atsz-52_y	Atlantic Source Zone	-67.4781	18.0319	20.00	85.87	56.30
atsz-52_z	Atlantic Source Zone	-67.5090	18.4529	20.00	85.87	39.20
atsz-53_a	Atlantic Source Zone	-68.4547	18.7853	20.00	83.64	22.10
atsz-53_b	Atlantic Source Zone	-68.5042	19.2048	20.00	83.64	5.00
atsz-53_y	Atlantic Source Zone	-68.3575	17.9463	20.00	83.64	56.30
atsz-53_z	Atlantic Source Zone	-68.4055	18.3658	20.00	83.64	39.20
atsz-54_a	Atlantic Source Zone	-69.6740	18.8841	20.00	101.54	22.10
atsz-54_b	Atlantic Source Zone	-69.5846	19.2976	20.00	101.54	5.00
atsz-55_a	Atlantic Source Zone	-70.7045	19.1376	20.00	108.19	22.10
atsz-55_b	Atlantic Source Zone	-70.5647	19.5386	20.00	108.19	5.00
atsz-56_a	Atlantic Source Zone	-71.5368	19.3853	20.00	102.64	22.10
atsz-56_b	Atlantic Source Zone	-71.4386	19.7971	20.00	102.64	5.00
atsz-57_a	Atlantic Source Zone	-72.3535	19.4838	20.00	94.20	22.10
atsz-57_b	Atlantic Source Zone	-72.3206	19.9047	20.00	94.20	5.00
atsz-58_a	Atlantic Source Zone	-73.1580	19.4498	20.00	84.34	22.10
atsz-58_b	Atlantic Source Zone	-73.2022	19.8698	20.00	84.34	5.00
atsz-59_a	Atlantic Source Zone	-74.3567	20.9620	20.00	259.74	22.10
atsz-59_b	Atlantic Source Zone	-74.2764	20.5467	20.00	259.74	5.00
atsz-60_a	Atlantic Source Zone	-75.2386	20.8622	15.00	264.18	17.94
atsz-60_b	Atlantic Source Zone	-75.1917	20.4306	15.00	264.18	5.00
atsz-61_a	Atlantic Source Zone	-76.2383	20.7425	15.00	260.70	17.94
atsz-61_b	Atlantic Source Zone	-76.1635	20.3144	15.00	260.70	5.00
atsz-62_a	Atlantic Source Zone	-77.2021	20.5910	15.00	259.95	17.94
atsz-62_b	Atlantic Source Zone	-77.1214	20.1638	15.00	259.95	5.00
atsz-63_a	Atlantic Source Zone	-78.1540	20.4189	15.00	259.03	17.94
atsz-63_b	Atlantic Source Zone	-78.0661	19.9930	15.00	259.03	5.00
atsz-64_a	Atlantic Source Zone	-79.0959	20.2498	15.00	259.24	17.94
atsz-64_b	Atlantic Source Zone	-79.0098	19.8236	15.00	259.24	5.00
atsz-65_a	Atlantic Source Zone	-80.0393	20.0773	15.00	258.85	17.94

Table 5. continued.

Segment	Description	Longitude (°E)	Latitude (°)	Strike (°)	Dip (°)	Depth (km)
atsz-65_b	Atlantic Source Zone	-79.9502	19.6516	15.00	258.85	5.00
atsz-66_a	Atlantic Source Zone	-80.9675	19.8993	15.00	258.60	17.94
atsz-66_b	Atlantic Source Zone	-80.8766	19.4740	15.00	258.60	5.00
atsz-67_a	Atlantic Source Zone	-81.9065	19.7214	15.00	258.51	17.94
atsz-67_b	Atlantic Source Zone	-81.8149	19.2962	15.00	258.51	5.00
atsz-68_a	Atlantic Source Zone	-87.8003	15.2509	15.00	62.69	17.94
atsz-68_b	Atlantic Source Zone	-88.0070	15.6364	15.00	62.69	5.00
atsz-69_a	Atlantic Source Zone	-87.0824	15.5331	15.00	72.73	17.94
atsz-69_b	Atlantic Source Zone	-87.2163	15.9474	15.00	72.73	5.00
atsz-70_a	Atlantic Source Zone	-86.1622	15.8274	15.00	70.64	17.94
atsz-70_b	Atlantic Source Zone	-86.3120	16.2367	15.00	70.64	5.00
atsz-71_a	Atlantic Source Zone	-85.3117	16.1052	15.00	73.70	17.94
atsz-71_b	Atlantic Source Zone	-85.4387	16.5216	15.00	73.70	5.00
atsz-72_a	Atlantic Source Zone	-84.3470	16.3820	15.00	69.66	17.94
atsz-72_b	Atlantic Source Zone	-84.5045	16.7888	15.00	69.66	5.00
atsz-73_a	Atlantic Source Zone	-83.5657	16.6196	15.00	77.36	17.94
atsz-73_b	Atlantic Source Zone	-83.6650	17.0429	15.00	77.36	5.00
atsz-74_a	Atlantic Source Zone	-82.7104	16.7695	15.00	82.35	17.94
atsz-74_b	Atlantic Source Zone	-82.7709	17.1995	15.00	82.35	5.00
atsz-75_a	Atlantic Source Zone	-81.7297	16.9003	15.00	79.86	17.94
atsz-75_b	Atlantic Source Zone	-81.8097	17.3274	15.00	79.86	5.00
atsz-76_a	Atlantic Source Zone	-80.9196	16.9495	15.00	82.95	17.94
atsz-76_b	Atlantic Source Zone	-80.9754	17.3801	15.00	82.95	5.00
atsz-77_a	Atlantic Source Zone	-79.8086	17.2357	15.00	67.95	17.94
atsz-77_b	Atlantic Source Zone	-79.9795	17.6378	15.00	67.95	5.00
atsz-78_a	Atlantic Source Zone	-79.0245	17.5415	15.00	73.61	17.94
atsz-78_b	Atlantic Source Zone	-79.1532	17.9577	15.00	73.61	5.00
atsz-79_a	Atlantic Source Zone	-78.4122	17.5689	15.00	94.07	17.94
atsz-79_b	Atlantic Source Zone	-78.3798	18.0017	15.00	94.07	5.00
atsz-80_a	Atlantic Source Zone	-77.6403	17.4391	15.00	103.33	17.94
atsz-80_b	Atlantic Source Zone	-77.5352	17.8613	15.00	103.33	5.00
atsz-81_a	Atlantic Source Zone	-76.6376	17.2984	15.00	98.21	17.94
atsz-81_b	Atlantic Source Zone	-76.5726	17.7278	15.00	98.21	5.00
atsz-82_a	Atlantic Source Zone	-75.7299	19.0217	15.00	260.15	17.94
atsz-82_b	Atlantic Source Zone	-75.6516	18.5942	15.00	260.15	5.00
atsz-83_a	Atlantic Source Zone	-74.8351	19.2911	15.00	260.83	17.94
atsz-83_b	Atlantic Source Zone	-74.7621	18.8628	15.00	260.83	5.00
atsz-84_a	Atlantic Source Zone	-73.6639	19.2991	15.00	274.84	17.94
atsz-84_b	Atlantic Source Zone	-73.7026	18.8668	15.00	274.84	5.00
atsz-85_a	Atlantic Source Zone	-72.8198	19.2019	15.00	270.60	17.94

Table 5. continued.

Segment	Description	Longitude (°E)	Latitude (°)	Strike (°)	Dip (°)	Depth (km)
atsz-85_b	Atlantic Source Zone	-72.8246	18.7681	15.00	270.60	5.00
atsz-86_a	Atlantic Source Zone	-71.9143	19.1477	15.00	269.06	17.94
atsz-86_b	Atlantic Source Zone	-71.9068	18.7139	15.00	269.06	5.00
atsz-87_a	Atlantic Source Zone	-70.4738	18.8821	15.00	304.49	17.94
atsz-87_b	Atlantic Source Zone	-70.7329	18.5245	15.00	304.49	5.00
atsz-88_a	Atlantic Source Zone	-69.7710	18.3902	15.00	308.94	17.94
atsz-88_b	Atlantic Source Zone	-70.0547	18.0504	15.00	308.44	5.00
atsz-89_a	Atlantic Source Zone	-69.2635	18.2099	15.00	283.88	17.94
atsz-89_b	Atlantic Source Zone	-69.3728	17.7887	15.00	283.88	5.00
atsz-90_a	Atlantic Source Zone	-68.5059	18.1443	15.00	272.93	17.94
atsz-90_b	Atlantic Source Zone	-68.5284	17.7110	15.00	272.93	5.00
atsz-91_a	Atlantic Source Zone	-67.6428	18.1438	15.00	267.84	17.94
atsz-91_b	Atlantic Source Zone	-67.6256	17.7103	15.00	267.84	5.00
atsz-92_a	Atlantic Source Zone	-66.8261	18.2536	15.00	262.00	17.94
atsz-92_b	Atlantic Source Zone	-66.7627	17.8240	15.00	262.00	5.00

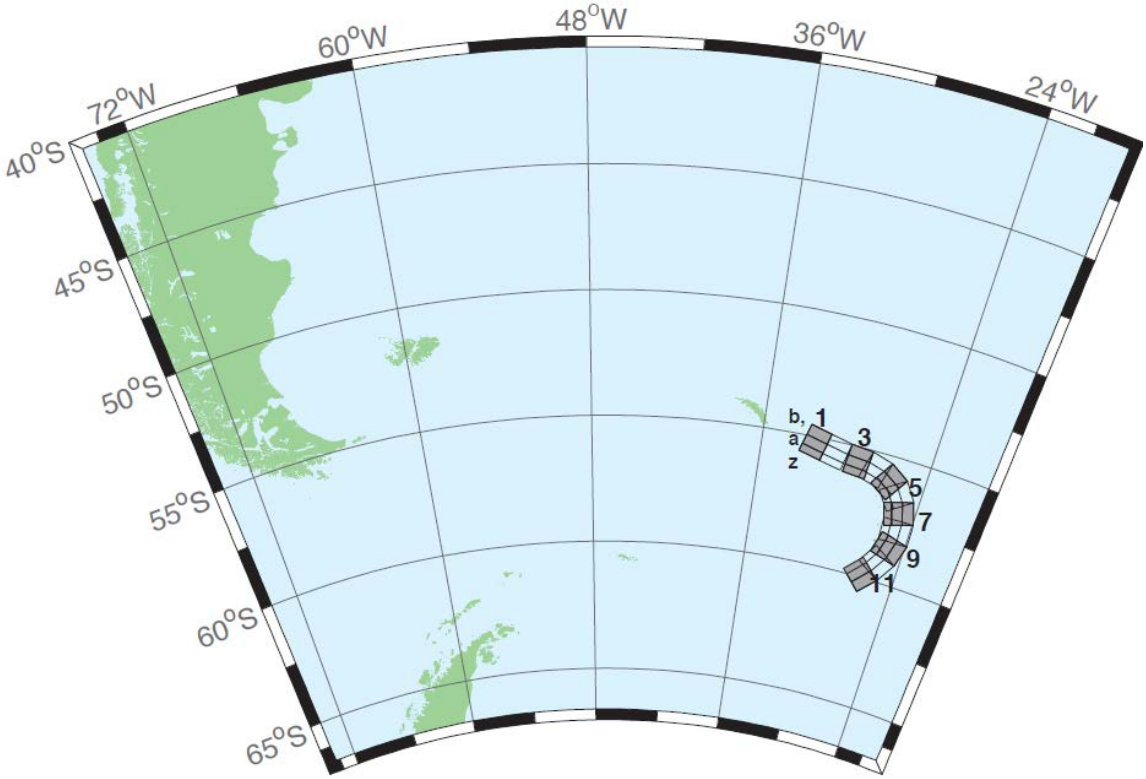

Figure 28. South Sandwich Islands Subduction Zone

Table 6. Earthquake parameters for South Sandwich Islands unit sources.

Segment	Description	Longitude (°E)	Latitude (°)	Strike (°)	Dip (°)	Depth (km)
sssz-01_a	South Sandwich Islands Subduction Zone	-32.3713	-55.4655	28.53	104.69	17.51
sssz-01_b	South Sandwich Islands Subduction Zone	-32.1953	-55.0832	9.96	104.69	8.87
sssz-01_z	South Sandwich Islands Subduction Zone	-32.5091	-55.7624	46.99	104.69	41.39
sssz-02_a	South Sandwich Islands Subduction Zone	-30.8028	-55.6842	28.53	102.45	17.51
sssz-02_b	South Sandwich Islands Subduction Zone	-30.6524	-55.2982	9.96	102.45	8.87
sssz-02_z	South Sandwich Islands Subduction Zone	-30.9207	-55.9839	46.99	102.45	41.39
sssz-03_a	South Sandwich Islands Subduction Zone	-29.0824	-55.8403	28.53	95.53	17.51
sssz-03_b	South Sandwich Islands Subduction Zone	-29.0149	-55.4469	9.96	95.53	8.87
sssz-03_z	South Sandwich Islands Subduction Zone	-29.1354	-56.1458	46.99	95.53	41.39
sssz-04_a	South Sandwich Islands Subduction Zone	-27.8128	-55.9796	28.53	106.14	17.51
sssz-04_b	South Sandwich Islands Subduction Zone	-27.6174	-55.5999	9.96	106.14	8.87
sssz-04_z	South Sandwich Islands Subduction Zone	-27.9659	-56.2744	46.99	106.14	41.39
sssz-05_a	South Sandwich Islands Subduction Zone	-26.7928	-56.2481	28.53	123.10	17.51
sssz-05_b	South Sandwich Islands Subduction Zone	-26.4059	-55.9170	9.96	123.10	8.87
sssz-05_z	South Sandwich Islands Subduction Zone	-27.0955	-56.5052	46.99	123.10	41.39
sssz-06_a	South Sandwich Islands Subduction Zone	-26.1317	-56.6466	23.28	145.62	16.11
sssz-06_b	South Sandwich Islands Subduction Zone	-25.5131	-56.4133	9.09	145.62	8.23
sssz-06_z	South Sandwich Islands Subduction Zone	-26.5920	-56.8194	47.15	145.62	35.87
sssz-07_a	South Sandwich Islands Subduction Zone	-25.6787	-57.2162	21.21	162.94	14.24
sssz-07_b	South Sandwich Islands Subduction Zone	-24.9394	-57.0932	7.60	162.94	7.63
sssz-07_z	South Sandwich Islands Subduction Zone	-26.2493	-57.3109	44.16	162.94	32.32
sssz-08_a	South Sandwich Islands Subduction Zone	-25.5161	-57.8712	20.33	178.21	15.91

Table 6. continued.

Segment	Description	Longitude (°E)	Latitude (°)	Strike (°)	Dip (°)	Depth (km)
sssz-08_b	South Sandwich Islands Subduction Zone	-24.7233	-57.8580	8.45	178.21	8.56
sssz-08_z	South Sandwich Islands Subduction Zone	-26.1280	-57.8813	43.65	178.21	33.28
sssz-09_a	South Sandwich Islands Subduction Zone	-25.6657	-58.5053	25.76	195.38	15.72
sssz-09_b	South Sandwich Islands Subduction Zone	-24.9168	-58.6128	8.25	195.38	8.54
sssz-09_z	South Sandwich Islands Subduction Zone	-26.1799	-58.4313	51.69	195.38	37.44
sssz-10_a	South Sandwich Islands Subduction Zone	-26.1563	-59.1048	32.82	212.51	15.65
sssz-10_b	South Sandwich Islands Subduction Zone	-25.5335	-59.3080	10.45	212.51	6.58
sssz-10_z	South Sandwich Islands Subduction Zone	-26.5817	-58.9653	54.77	212.51	42.75
sssz-11_a	South Sandwich Islands Subduction Zone	-27.0794	-59.6799	33.67	224.24	15.75
sssz-11_b	South Sandwich Islands Subduction Zone	-26.5460	-59.9412	11.33	224.24	5.93
sssz-11_z	South Sandwich Islands Subduction Zone	-27.4245	-59.5098	57.19	224.24	43.46

Appendix C Description of Indices

This report makes use of six indices to estimate the degree of agreement between the reference and forecast model. Allen and Greenslade (2012) investigated the suitability of these indices for the objective assessment of tsunami models.

In formulating the indices, we take a series of form the reference model denoted R, which consists of n time-ordered elements $\{R_1, R_2, \ldots, R_n\}$. We take an equivalent time series form the forecast model, which we denote F and which we wish to test against R. The series F will also consist of n time-ordered elements $\{F_1, F_2, \ldots, F_n\}$ such that each element in F corresponds, with respect to time, to an element in R. Both of these series start from some time that is defined here to be when either of the two series first exceeds a threshold of 1cm (except for the micro scenario and scenario 7, where this threshold is set to 0.1 cm).

C.1 Normalized error in the maximum amplitude

In forecast and warning applications, knowledge of the largest expected wave is often sought. In that regard, we would seek to minimise errors in the maximum (positive) forecast amplitude. This index, $\varepsilon_{\max}$, is made non-dimensional by normalising by the observed maximum amplitude:

$$\varepsilon_{\max} = \frac{F_{\max} - R_{\max}}{R_{\max}}$$

where $R_{\max}$ is the maximum value of the reference model time series, and similarly, $F_{\max}$ is the maximum value of the forecast model time series. This index has no upper bound, but has a lower bound of -1 when $R_{\max}$ is much larger than $F_{\max}$ and under the reasonable assumption that both $R_{\max}$ and $F_{\max}$ are both positive. A perfect estimation by the forecast model of the maximum amplitude is indicated by a value of zero. Given this, over- or under-prediction of the maximum Reference model value is denoted by negative and positive values, respectively.

C.2 Pearson correlation coefficient

The Pearson correlation coefficient, r, is a measure that is widely used to reveal relationships between two time series. Given the mean and standard deviations of the observed series, $\bar{R}$ and σ_R respectively, and the same for the predicted series, $\bar{F}$ and σ_F, the coefficient is calculated for a time series of n-elements in length by

$$r = \frac{1}{n-1}\sum_{i=1}^{n}\frac{\left(P_i - \bar{P}\right)}{\sigma_P}\frac{\left(O_i - \bar{O}\right)}{\sigma_O}$$

The coefficient is bounded over [-1, 1], with 1 indicating a perfect linear relationship between the forecast and reference model time series, and -1 indicating a perfect, but inverse linear relationship. It should be noted that this index does not take into account differences in variance between the two series.

C.3 Normalized Root-mean-square error

The root-mean-square error, RMSE, is another common index used to assess model performance. It is essentially a measure of the mean deviation of the forecast model time series from the reference model time series. Normalised RMSE used here is:

$$\mathrm{nRMSE} = \frac{1}{\sigma_R}\sqrt{\frac{1}{n}\sum_{i=1}^{n}\left(F_i - R_i\right)^2}$$

Values of RMSE have a minimum value of 0, indicating perfect agreement (or zero error), but no upper bound.

C.4 Index of Agreement

Willmott (1981) devised a complementary index to RMSE that aims to specify "the degree to which the observed (i.e. reference model time series) deviations about $\bar{R}$ correspond, both in magnitude and sign, to the predicted (forecast) deviations about $\bar{R}$" (Willmott, 1981). Following further refinements by Willmott et al. (1985), this Index of Agreement, IOA, is formulated as:

$$\mathrm{IOA} = 1 - \frac{\sum_{i=1}^{n}\left|F_i - R_i\right|}{\sum_{i=1}^{n}\left(\left|F_i - \bar{R}\right| + \left|R_i - \bar{R}\right|\right)}$$

Willmott (1981) described this ratio as being a comparison between the mean absolute deviation and the mean potential error. The values of this index are bounded between 0 and 1, with 1 indicating perfect agreement between the forecast and reference models.

C.5 Watterson's transformed Mielke index

Watterson (1996) made a geometric argument to transform an index by Mielke (1984) (similar to the Mielke and Berry (2001) index below). His adaption means the index is bounded over [-1,1], with perfect agreement again indicated by a value of 1. It is formulated by:

$$M = \tfrac{2}{\pi}\sin^{-1}\left(1 - \frac{\mathrm{MSE}}{\sigma_F^2 + \sigma_R^2 + \left(\bar{F} - \bar{R}\right)^2}\right)$$

where

$$\mathrm{MSE} = \tfrac{1}{n}\sum_{i=1}^{n}\left(F_i - R_i\right)^2$$

is the mean square error.

C.6 Mielke and Berry index

The index of Mielke and Berry (2001) is more accurately described as the Multiresponse Randomized Block Procedure (MRBP). It compares the mean absolute deviation to a measure comprised of the sum of the permutations of the deviation of each prediction from each observation.

$$\Re = 1 - \frac{\tfrac{1}{n}\sum_{i=1}^{n}\left|F_i - R_i\right|}{\tfrac{1}{n^2}\sum_{i=1}^{n}\sum_{j=1}^{n}\left|F_j - R_i\right|}$$

Predictions that are in perfect agreement with the observations give this index an upper bound of 1. Mielke and Berry (2001) state that for n > 2, this index has a lower bound of -0.5.

Appendix D. SIFT Testing

Forecast models are tested with synthetic tsunami events covering a range of tsunami source locations and magnitudes. Testing is also done with selected historical tsunami events when available.

The purpose of forecast model testing is three-fold. The first objective is to assure that the results obtained with the NOAA's tsunami forecast system software, which has been released to the Tsunami Warning Centers for operational use, are consistent with those obtained by the researcher during the development of the forecast model. The second objective is to test the forecast model for consistency, accuracy, time efficiency, and quality of results over a range of possible tsunami locations and magnitudes. The third objective is to identify bugs and issues in need of resolution by the researcher who developed the Forecast Model or by the forecast system software development team before the next version release to NOAA's two Tsunami Warning Centers.

Local hardware and software applications, and tools familiar to the researcher(s), are used to run the Method of Splitting Tsunamis (MOST) model during the forecast model development. The test results presented in this report lend confidence that the model performs as developed and produces the same results when initiated within the forecast system application in an operational setting as those produced by the researcher during the forecast model development. The test results assure those who rely on the Bar Harbor tsunami forecast model that consistent results are produced irrespective of system.

D.1. TESTING PROCEDURE

The general procedure for forecast model testing is to run a set of synthetic tsunami scenarios and a selected set of historical tsunami events through the forecast system application and compare the results with those obtained by the

researcher during the forecast model development and presented in the Tsunami Forecast Model Report. Specific steps taken to test the model include:

1. Identification of testing scenarios, including the standard set of synthetic events, appropriate historical events, and customized synthetic scenarios that may have been used by the researcher(s) in developing the forecast model.
2. Creation of new events to represent customized synthetic scenarios used by the researcher(s) in developing the forecast model, if any.
3. Submission of test model runs with the forecast system, and export of the results from A, B, and C grids, along with time series.
4. Recording applicable metadata, including the specific forecast system version used for testing.
5. Examination of forecast model results for instabilities in both time series and plot results.
6. Comparison of forecast model results obtained through the forecast system with those obtained during the forecast model development.
7. Summarization of results with specific mention of quality, consistency, and time efficiency.
8. Reporting of issues identified to modeler and forecast system software development team.
9. Retesting the forecast models in the forecast system when reported issues have been addressed or explained.

Synthetic model runs were tested on a DELL PowerEdge R510 computer equipped with two Xeon E5670 processors at 2.93 GHz, each with 12 MBytes of cache and 32GB memory. The processors are hex core and support hyper-threading, resulting in the computer performing as a 24 processor core machine. Additionally, the testing computer supports 10 Gigabit Ethernet for fast network connections. This computer configuration is similar or the same as the configurations of the computers installed at the Tsunami Warning Centers so the compute times should only vary slightly.

D.2 Results

The Bar Harbor forecast model was tested with SIFT version 3.2.

The Bar Harbor, Maine forecast model was tested with three synthetic scenarios. Test results from the forecast system and comparisons with the results obtained during the forecast model development are shown numerically in Table 7 and graphically in Figures 29 to 31. The results show that the minimum and maximum amplitudes and time series obtained from the forecast system agree with those obtained during the forecast model development, and that the forecast model is stable and robust, with consistent and high quality results across geographically distributed tsunami sources. The model run time (wall clock time) was 58.0 minutes for 12 hours of simulation time, and 19.3 minutes for 4.0 hours. This run time is not within the 10 minute run time for 4 hours of simulation time and does not satisfy run time requirements. This is attributed to the grid resolution used in the forecast model. Meeting the 10 minute run for a 4 hour of tsunami simulation would require a coarser grid resolution or smaller grid coverage or both. Both options are not recommended since a coarse grid resolution would capture fewer nodes per tsunami wave length thus not resolving it properly and smaller grid coverage would not be able to capture the wave interaction with the islands in its surrounding area.

A suite of three synthetic events was run on the Bar Harbor forecast model. The modeled scenarios were stable for all cases run. The largest modeled tsunami wave amplitude was 150 centimeters (cm) from the Atlantic (ATSZ 48-57) source zone. The smallest signal of 13 cm was recorded at the far field South Sandwich (SSSZ 01-10) source zone. Comparisons between the development cases and the forecast system output were consistent in shape and amplitude for all cases run. The Bar Harbor reference point used for the forecast model development is the same as what is deployed in the forecast system, so the results can be considered valid for the three cases studied.

Table 7. table of maximum and minimum amplitudes (cm) at the Bar harbor, Maine warning point for synthetic events tested using SIFT 3.2 and obtained during development.

Scenario Name	Source Zone	Tsunami Source	α [m]	SIFT Max (cm)	Development Max (cm)	SIFT Min (cm)	Development Min (cm)
Mega-tsunami Scenarios							
ATSZ 35-44[1]	Atlantic	A38-A47, B38-B47	25	78.2		-90.6	
ATSZ 48-57	Atlantic	A48-A57, B48-B57	25	150.1	150.1	-209.0	-203.0
SSSZ 1-10	South Sandwich	A1-A10, B1-B10	25	12.6	12.6	-13.9	-13.9

[1] This was not part of the development tests

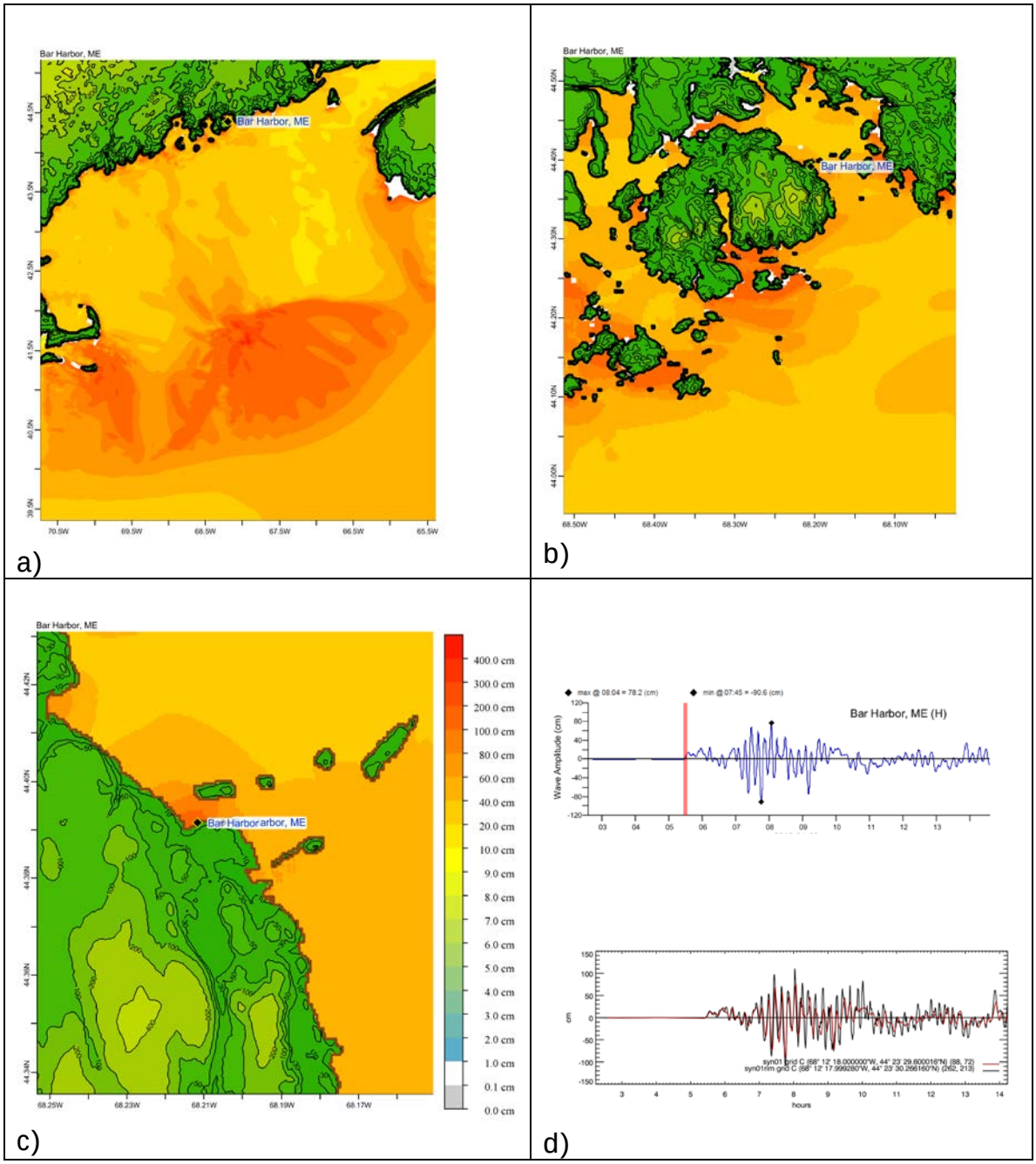

Figure 29: Response of the Bar Harbor forecast model to synthetic scenario ATSZ 38-47 (alpha=25). Maximum sea surface elevation for (a) A-grid, b) B-grid, c) C-grid. Sea surface elevation time series at the C-grid warning point (d) The lower time series plot is the result obtained during model development and is shown for comparison with test results.

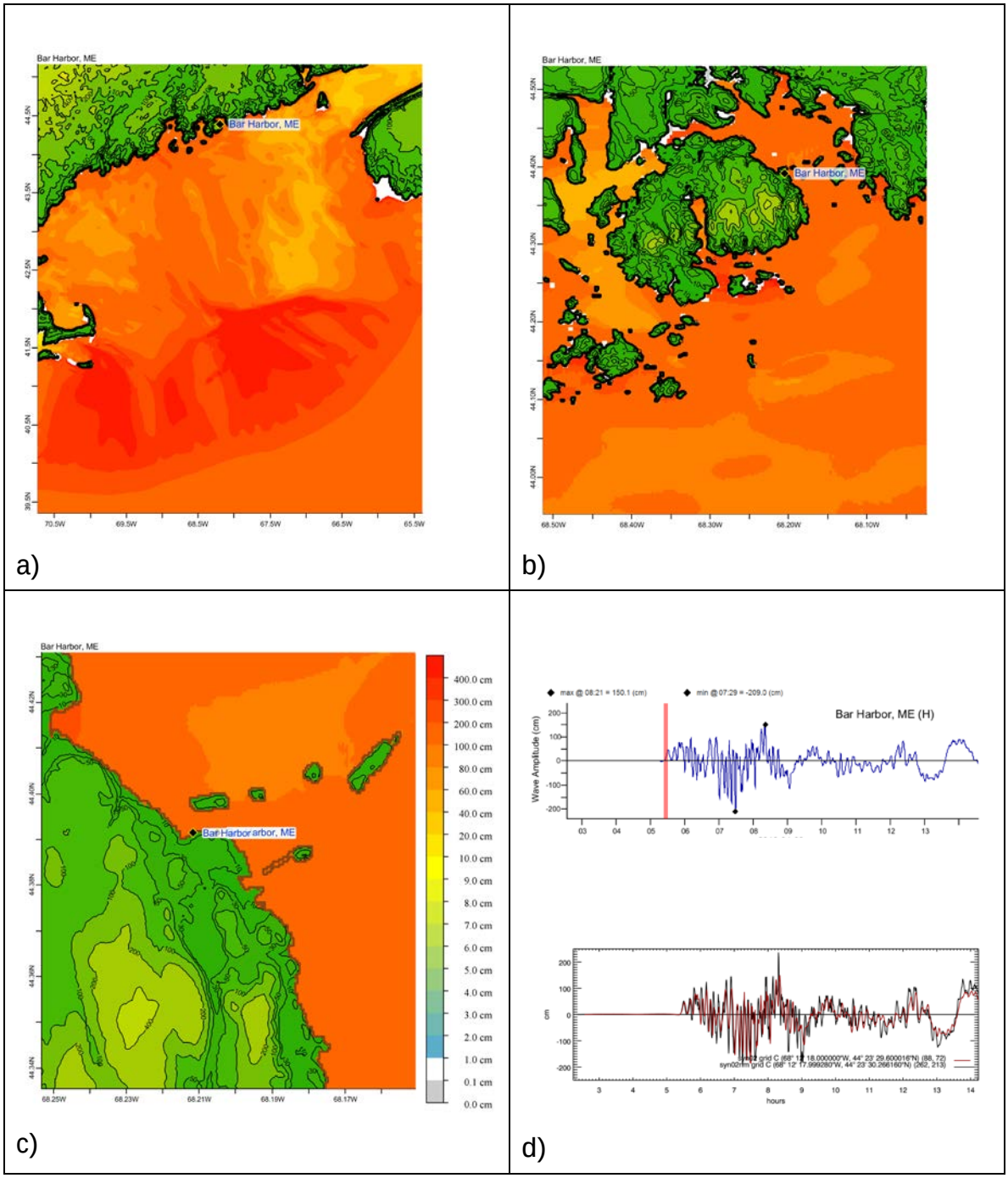

Figure 30: Response of the Bar Harbor forecast model to synthetic scenario ATSZ 48-57 (alpha=25). Maximum sea surface elevation for (a) A-grid, b) B-grid, c) C-grid. Sea surface elevation time series at the C-grid warning point (d) The lower time series plot is the result obtained during model development and is shown for comparison with test results.

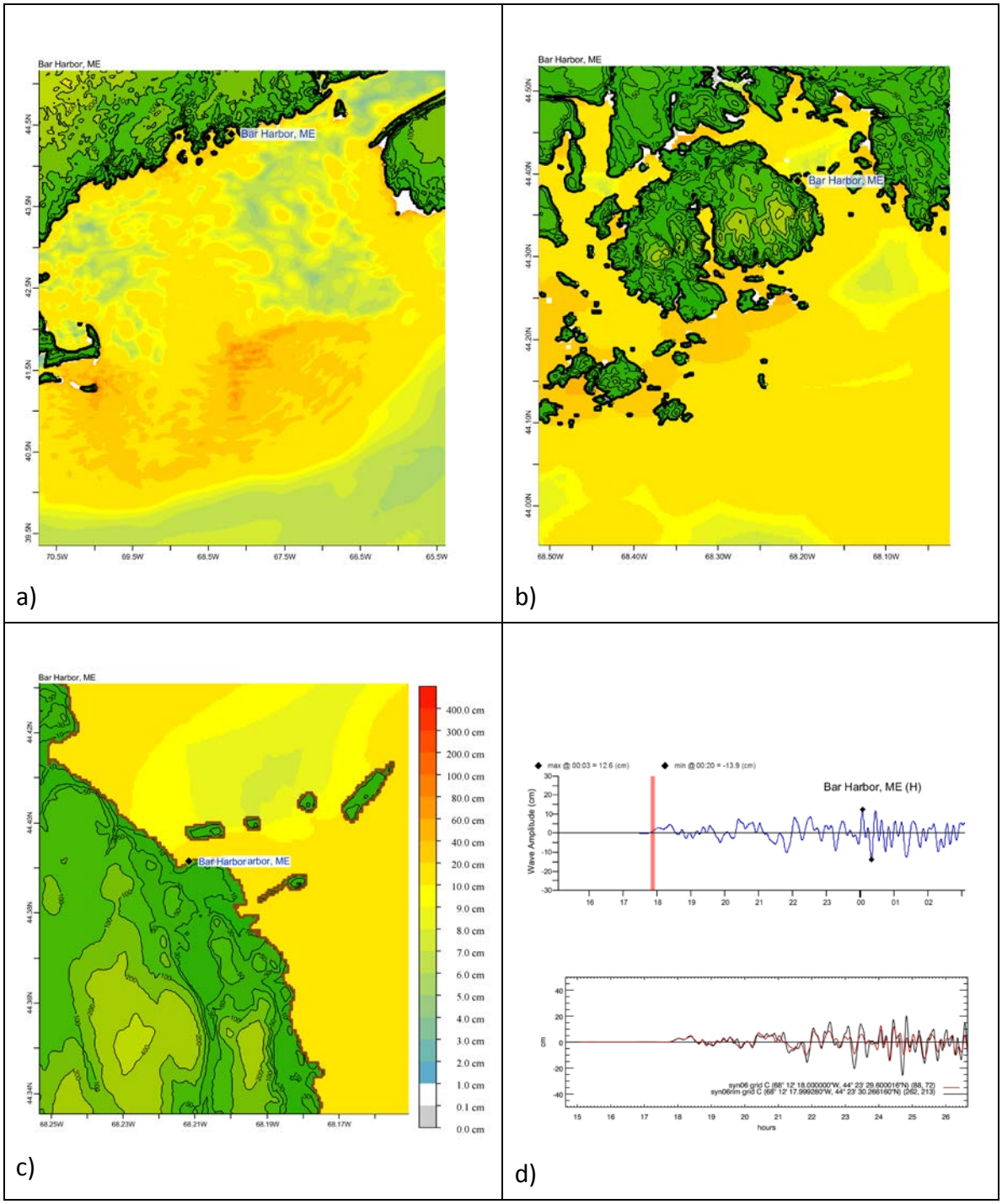

Figure 31: Response of the Bar Harbor forecast model to synthetic scenario SSSZ 1-10 (alpha=25). Maximum sea surface elevation for (a) A-grid, b) B-grid, c) C-grid. Sea surface elevation time series at the C-grid warning point (d) The lower time series plot is the result obtained during model development and is shown for comparison with test results.